

Finite size effect on dynamical entanglement entropy: CFT and holography

Gautam Mandal^{a,1}, Ritam Sinha^{a,2}, and Tomonori Ugajin^{b,3}

^a*Department of Theoretical Physics
Tata Institute of Fundamental Research, Mumbai 400005, India.*

^b*Kavli Institute for Theoretical Physics, University of California,
Santa Barbara, CA 93106, USA*

Abstract

Time-dependent entanglement entropy (EE) is computed for a single interval in two-dimensional conformal theories from a quenched initial state in the presence of spatial boundaries. The EE is found to be periodic in time with periodicity equal to the system size L . For large enough L , the EE shows a rise to a thermal value (characterized by a temperature $1/\beta$ determined by the initial state), followed by periodic returns to the original value. This works irrespective of whether the conformal field theory (CFT) is rational or irrational. For conformal field theories with a holographic dual, the large c limit plays an essential role in ensuring that the EE computed from the CFT is universal (independent of the details of the CFT and of boundary conditions) and is exactly matched by the holographic EE. The dual geometry is computed and it interpolates between a BTZ black hole at large L and global AdS at large β .

¹e-mail: mandal@theory.tifr.res.in

²sinha@theory.tifr.res.in

³ugajin@kitp.ucsb.edu

Contents

1	Introduction and Summary	2
2	CFT with finite spatial boundary	4
2.1	Mapping the rectangle to the upper half plane	5
2.2	One Point Function	7
2.2.1	Analytic continuation to real time correlators	8
2.3	Behavior of the Energy density	9
2.3.1	Time-dependence	9
2.3.2	Space dependence: Localized thermal region	10
2.4	Thermalization and ‘revival’ of a local operator	11
3	Evolution of entanglement entropy following a quench	12
3.1	Method of Images	13
3.2	Large L/β limit	14
3.3	Low temperature (L/β small)	15
3.4	Universality of the Entanglement Entropy at large central charge	15
3.4.1	At Low Temperature	15
3.4.2	For All Temperatures	17
4	Bulk dual	18
4.1	Holographic quantum quench and entanglement entropy	21
4.2	Evolution of holographic entanglement entropy	23
4.2.1	Time periodicity of two-point functions and the hEE	24
4.2.2	Low temperature limit $\frac{L}{\beta} \rightarrow 0$	25
4.2.3	Large L limit $\frac{L}{\beta} \rightarrow \infty$	25
5	The quasiparticle picture of the evolution of the entanglement entropy	26
5.1	The quasiparticle interpretation for global quench for infinite spatial size	26
5.2	The evolution of entanglement entropy in the presence of boundaries	27
5.3	$\frac{l}{L} > \frac{1}{2}$	27
5.4	$\frac{l}{L} < \frac{1}{2}$	28
6	Conclusion	30
A	Derivation of conformal maps	31
A.1	Map from the rectangle to the complex plane (Euclidean)	31
A.2	Lorentzian map	34
A.3	A different Euclidean map	35
B	Decay rate in the high temperature limit	36

1 Introduction and Summary

Quantum quench refers to non-equilibrium dynamics caused by a sudden change of the Hamiltonian. Interest in studies of this phenomenon has partly been spurred by its experimental realization in cold atom systems. The pioneering article [1] by Greiner et al addressed the question of a quantum phase transition following a quantum quench in a system of ultracold atoms. Theoretical interest has also grown in this area following seminal work on quantum quenches involving conformal and integrable models, especially in two dimensions [2, 3]. An important question addressed in these studies is whether a closed dynamical system, following a quantum quench, approaches a thermal equilibrium. For conformal field theories with a holographic dual, this question takes an independently interesting meaning, since the holographic dual of thermalization turns out to be gravitational collapse to a black hole [4, 5, 6].

In two dimensions, with infinite spatial size, quantum quench to a critical point has been discussed extensively by Calabrese and Cardy in a series of papers, starting with [7, 8]. The final hamiltonian in this problem corresponds to a 2D CFT and the quenched state is effectively replaced, at least for the physics of long wavelengths, by a simpler choice of initial wavefunction which is a conformal boundary state with a UV cutoff scale. Such states are translationally invariant, and the quench is called a global quench. The post-quench time evolution of various observables is given by path integrals on a strip whose width is determined by the cut-off scale. Local observables confined within an interval can be shown to thermalize at rates with universal properties [9]. This happens even in the presence of arbitrary number of conserved charges, e.g., for integrable CFTs where the thermal ensemble is given by a generalized Gibbs ensemble (GGE) [10, 11]. In a holographic context, the thermalization in the CFT matches the decay of quasinormal modes [12] of black holes (in case of the GGE, it corresponds to quasinormal modes of the higher spin black hole [10]). Another important time-dependent observable in the CFT is the entanglement entropy (EE); this was first calculated in the article [8] in the quench model of [7] where the growth of entanglement was also given an interpretation in terms of quasiparticles moving at the speed of light (for a recent work on a bound on the spread of entanglement, see [13]). In a holographic context, the time-dependent EE of [8] has been matched with computations in black hole geometries [14] (see also [15]).

The above discussions have been generalized to introduce inhomogeneities in the initial state by applying a conformal transformation, in which case time evolution of various observables can be understood in terms of path integrals on appropriate inhomogeneous strips [16]. A holographic dual of this set up was studied in [17], and in a related context involving the eternal black hole, in [18]. Other work in this regard includes studies of local quenches in various contexts, see, e.g. [19, 20, 21, 22].

In much of the above discussion, the spatial extent of the system is infinite (or much larger than any other length scale in the problem). The effect of a finite spatial extent on thermalization has been a topic of long interest, e.g. in the context of the FPU problem [23, 24, 25]. From the point of view of experimental realizations, in case of 2D CFT's, the spatial boundaries can be thought of as representing impurities in a quantum critical system. Thermalization, or lack thereof, for global quenches in a finite system of length L has recently been studied in [9], where it has been shown that for rational CFT's, the quenched state returns to itself after a finite period of time which is a multiple of $L/2$. The reason for this 'revival' was roughly that the time-dependence of the wavefunction, for rational highest weights, is a sum of terms with rational periods. Correlation functions and entanglement entropy of subsystems also follow a periodic behaviour. The periodic behaviour of entanglement entropy was explicitly confirmed in the global quench on a circle for free fermions in [26]. In [27], the periodic behaviour observed in [9] is explained by interpreting the quenched state in terms of a Lorentzian-signature conformal transformation of the ground state on the strip; this paper also comments on a holographic formulation. For other discussions on quenches on the segment, we refer to [28, 29, 30] and the recent discussion [31]. Revival in higher dimensional field theories has been considered in [32]; holographic entanglement entropy has also been discussed in 2+1 dimensional systems with finite size [33] where a partial revival has been found.

The main focus of our paper will be to study the effect of finite system size on various time-dependent phenomena. Below we summarize the contents and main results of our paper:

(i) We study time evolution of observables in a 2-dimensional CFT starting from a quenched state with a UV cutoff scale $1/\beta$ (as described above) in the presence of finite spatial boundaries (with system size L). The tool used in the CFT computations is a conformal map (the Christoffel-Schwarz transformation), as in [27], which converts a rectangular geometry to an upper half plane (see Section 2.1 and Appendix A). The map gets simplified in the limits of large L and large β respectively and can be identified with known versions of the map from a cylinder to a plane.

(ii) We show that the spatial boundaries lead to locally thermalized regions (characterized by a *temperature* $1/\beta$) which merge and split periodically at regular time intervals given by the system size. We also quantitatively compute thermalization of certain observables on intermediate time scales prior to the occurrence of the 'revival' phenomena discussed above. We show that in the limit of large L , the relaxation rate agrees with the known results for infinite systems (see Sections 2.2, 2.3, 2.4 and Appendix B). Part of the above discussion has already appeared in [27, 30] (see also [31]).

(iii) In Section 4 we present a bulk dual of the CFT on a rectangle, following the AdS/CFT proposal for CFT with boundaries [34, 35, 36, 37, 38], coupled with [39, 17, 18] which discuss a *large diffeomorphism* (see Eqn. (56)) that reduce to the (analytically con-

tinued) conformal map discussed above. The periodicity of various observables mentioned above can be interpreted in terms of the time-periodicity of the above large diffeomorphism, which effects a time-periodic change of the (regulated) AdS boundary and, in turn, causes such changes in geometric quantities such as lengths of geodesics tied to the boundary.

(iv) The main results of our paper, presented in Sections 3, 4 and 5, concern the computation of the entanglement entropy (EE) of a single interval of length l . We use the conformal map described above, and the method of images, to relate the CFT computation of EE to a four-point function of ‘twist operators’ on the plane. We also compute the EE using holographic methods (Section 4.1), developing on earlier work by one of the authors [17]. The holographic result is universal and does not depend on the specific CFT (except on the central charge). The CFT result, on the other hand, involves a four-point function which generically depends on the specific CFT. At large L , the CFT four-point function factorizes, becomes universal, and readily agrees with the holographic result. The analysis for general L/β , however, is much more subtle; we show that (see Section 3.4), although the CFT four-point function does not *a priori* factorize, it takes a universal form provided one takes an appropriate large c limit discussed recently [40, 19, 41, 42]. We show that this new universal form then agrees with the result obtained from holography.

(vi) Another novel computation of our paper (see Section 5) is that of the EE by adapting the quasiparticle method [8] to the presence of spatial boundaries. The boundaries leads to hard wall reflection of the quasiparticles, causing periodic entry and exit of EPR partners to and from the interval of interest. We compute the resulting entanglement entropy. The result quantitatively agrees with the large L results discussed in the last paragraph.

(vii) We should remark that in [9], revival was investigated by using the fidelity function $|\langle \psi_0 | \exp[-iHt] \psi_0 \rangle|^2$ ⁴; it was pointed out that no such revival was expected in the presence of a continuum of (or more generally, incommensurate) conformal weights, e.g. in an irrational conformal field theory. The periodicity we find in this paper in entanglement entropy and other observables is observed, however, in *any* CFT, including large c theories with a holographic dual. This is tied to the fact that these observables are not sufficient to distinguish between rational and irrational theories; see [31] for a recent discussion.

2 CFT with finite spatial boundary

In this section, we will describe quantum quench in the presence of a spatial boundary using conformal field theory methods. We will review some known results [9, 27] and some new results for time-dependent one-point functions. We will discuss CFT computation of EE in the next section.

We will consider spatial boundaries at $x = \pm L/2$, and following [8], an initial state of

⁴This is a simpler version of the so-called Loschmidt echo.

the form,

$$|\psi_0\rangle = e^{-\beta H/4}|B\rangle. \quad (1)$$

where the state $|B\rangle$ is a conformal boundary state (the state $|\psi_0\rangle$ can be regarded as an approximation to a realistic quench state [43, 44, 45]). The parameter β can be regarded as a length scale which cuts off the UV modes to render the state normalizable.⁵ Following [8], we will view this wavefunction as the result of a Euclidean time evolution from a boundary state $|B\rangle$ at $\tau = -\beta/4$ to $|\psi_0\rangle$ at $\tau = 0$. Real time evolution of (1) is described by continuing τ to complex values:

$$|\psi(t)\rangle = e^{-iHt}|\psi_0\rangle = e^{-\tau H}|B\rangle, \quad \tau = \beta/4 + it. \quad (2)$$

We would be interested in time-dependent quantities such as (a) the equal-time correlators

$$\langle O_1(x_1, t) \dots O_n(x_n, t) \rangle \equiv \langle \psi(t) | O_1(x_1) \dots O_n(x_n) | \psi(t) \rangle. \quad (3)$$

or (b) the entanglement entropy $S_{EE}(t)$ of an interval $A = [-l/2, l/2]$ when the system as a whole is described by the wavefunction (2). As discussed in [8] (see below), $S_{EE}(t)$ is related to a two-point correlator of the above kind.

As mentioned above, the boundary state $|B\rangle$ implements a certain boundary condition on the time boundary $\tau = -\beta/4$. When the *same* boundary conditions are also imposed at the spatial boundaries $x = \pm L/2$, then the correlators (3) can be evaluated by a functional integral over a rectangle (see figure 1), with boundary condition relevant to the boundary state $|B\rangle$ imposed on all sides of the rectangle.⁶

2.1 Mapping the rectangle to the upper half plane

Functional integrals over a rectangular region are not easy to compute directly. However, since we are dealing with a CFT, and the boundary conditions do not break conformal symmetry, the CFT correlators (3) are covariant under conformal transformations. We can thus reduce the computation to that on the upper half plane (UHP) by using a conformal map from the rectangle to the UHP. The necessary map for this purpose is a Christoffel-Schwarz transformation⁷, defined by

$$w(z) = A \int_0^z \frac{dz}{\sqrt{(z^2 - b^2)(z^2 - \frac{1}{b^2})}} + B, \quad (4)$$

⁵We will find below that for large enough L/β , the energy of this state coincides with the energy of a thermal ensemble characterized by an inverse temperature β (see (20)). Hence, from here on we will refer to $1/\beta$ as a ‘temperature’, although we should remember that we are still dealing with a pure state and the nomenclature is only a formal one.

⁶In case the spatial boundary conditions are different from the temporal boundary conditions, one needs to insert some boundary operators at the corners of the rectangle [46].

⁷The transformation we use here is a little different from that found in literature. The reason is that we want to explore both the low and the high values of L/β using this map by simply tuning the parameter b .

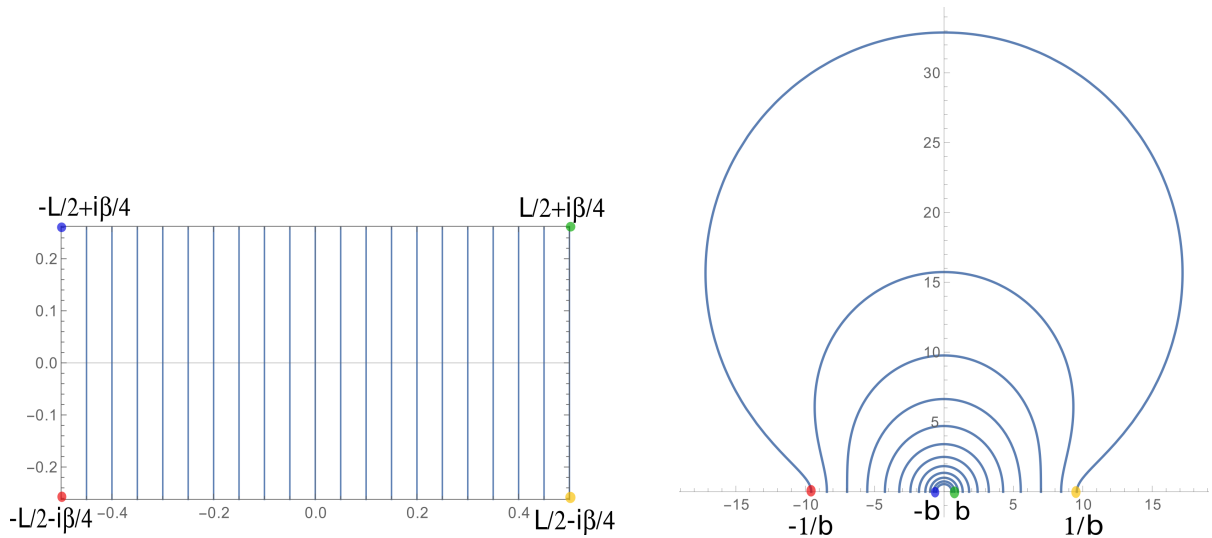


Figure 1: Maps between the upper half plane and the rectangle. The colour coding represents the mapping of the corners to the boundary of the UHP. See (88) and (87). The time evolution contours in the rectangle are mapped to the UHP as shown on the right. We have chosen $L = \beta = 1$.

Here, z is a complex coordinate on the UHP (defined by the region $\text{Im}(z) \geq 0$ of the plane), whereas $w = x + i\tau$ is a complex coordinate parametrizing the above-mentioned rectangular region (bounded by the lines $|\text{Re}(w)| \leq L/2$, $|\text{Im}(w)| \leq \beta/4$, see figure 1). A, B are constants which determine the images of the corners of the rectangle on the boundary of the UHP. Without loss of generality, the four image points can be chosen to have z -coordinates: $(z_1, z_2, z_3, z_4) = (-1/b, -b, b, 1/b)$ with $(0 \leq b \leq 1)$. We will look for a map which sends these points to the following corners of the rectangle respectively:

$$w\left(-\frac{1}{b}\right) = -\frac{L}{2} - i\frac{\beta}{4}, \quad w(-b) = -\frac{L}{2} + i\frac{\beta}{4}, \quad w(b) = \frac{L}{2} + i\frac{\beta}{4}, \quad w\left(\frac{1}{b}\right) = \frac{L}{2} - i\frac{\beta}{4}. \quad (5)$$

The required map is discussed in [27] (see also Appendix A). For convenience, we reproduce here the map $z(w)$ (88) from the rectangle to the UHP

$$z(w) = b \operatorname{sn} \left[\frac{4K(b^4)}{i\beta} \left(w - \frac{L}{2} \right), b^4 \right], \quad \bar{z}(\bar{w}) = b \operatorname{sn} \left[\frac{4K(b^4)}{-i\beta} \left(\bar{w} - \frac{L}{2} \right), b^4 \right]. \quad (6)$$

The parameter b determines the aspect ratio of the rectangle:

$$\frac{\beta}{L} = \frac{4K(b^4)}{K(1-b^4)}. \quad (7)$$

We show in Appendix A that the map (6) can also be regarded as a map from the torus (a product of two circles of sizes $2L, \beta$) owing to the periodicity properties (91). The map also has a large L limit (96)

$$z(w) = i \exp[-2\pi w/\beta], \quad (8)$$

and a low temperature⁸ limit (97)

$$z(w) = i \cot \left(\frac{\pi}{4} + \frac{\pi w}{2L} \right). \quad (9)$$

2.2 One Point Function

In this section, we will evaluate a one-point function $\langle O(x, t) \rangle$ as defined in (3) (part of the above discussion has already appeared in [27, 30], see also [31]). The evaluation would include calculating the one point function in Euclidean time τ and then analytically continuing to Lorentzian time t . We shall however, first, use the map $z(w)$ (6) to relate the one-point function on the rectangle to that on the UHP.

Primary operators For a primary operator $O(w, \bar{w})$, of dimension (h, \bar{h}) , the one-point function on the rectangle becomes

$$\langle O(w, \bar{w}) \rangle_{\text{rect}} = \left(\frac{\partial z}{\partial w} \right)^h \left(\frac{\partial \bar{z}}{\partial \bar{w}} \right)^{\bar{h}} \langle O(z, \bar{z}) \rangle_{\text{UHP}}. \quad (10)$$

For a holomorphic operator, or an operator with $\bar{h} \neq h$, the above one-point function on the UHP vanishes. However, for a primary operator of the form $O_{h,h}(w, \bar{w}) = \phi_h(w) \phi_h^\dagger(\bar{w})$, (with $\bar{h} = h$)⁹ the above one-point function on the UHP is non-zero and is given by the ‘method of images’ [46]. According to this method, the conformal boundary condition on the UHP amounts to replacing the antiholomorphic operator $\phi_h^\dagger(\bar{z})$ from the point $P = (z, \bar{z})$ by a holomorphic operator $\phi_h(z')$ at the image point $P' = (z', \bar{z}')$ (with $z' = \bar{z}, \bar{z}' = z$). The one-point function is now given by the holomorphic 2-point function on the plane¹⁰

$$\langle O_{h,h}(P) \rangle_{\text{UHP}} = A_b \langle \phi_h(P) \phi_h^\dagger(P') \rangle_{\mathbb{C}} = A_b \langle \phi_h(z) \phi_h^\dagger(z') \rangle_{\mathbb{C}}$$

Hence, the original one-point function, for primary operators $O_{h,h}(w, \bar{w}) \equiv \phi_h(w) \phi_h^\dagger(\bar{w})$ reduces to

$$\langle O_{h,h}(w, \bar{w}) \rangle_{\text{rect}} = \left(\frac{\partial z}{\partial w} \right)^h \left(\frac{\partial \bar{z}}{\partial \bar{w}} \right)^h \langle \phi_h(z) \phi_h^\dagger(z') \rangle_{\mathbb{C}} \quad (11)$$

Quasiprimary operators In case the operator $O(w, \bar{w})$ is quasiprimary, it mixes with lower dimension operators under conformal transformations, leading to additional terms

⁸We use the word ‘temperature’ to refer to $1/\beta$ in the sense of footnote 5.

⁹Here we allow for complex operators ϕ ; ϕ^\dagger denotes the hermitian conjugate.

¹⁰Up to a constant A_b which depends on the operator O and the boundary state $|B\rangle$. We will assume that $A_b \neq 0$; the precise value of this constant will be unimportant and we will drop it henceforth.

in (10). For example, for the holomorphic stress tensor $T(w) \equiv T_{ww}(w)$, the conformal transformation to the UHP is given by

$$\langle T(w) \rangle_{\text{rect}} = \left(\frac{\partial z}{\partial w} \right)^2 \langle T(z) \rangle_{\text{UHP}} - \frac{c}{12} \{z, w\} = -\frac{c}{12} \{z, w\} \quad (12)$$

In the second equality we have used the fact that $\langle T(z) \rangle$ on the UHP is the same as that on the plane (since it does not have an antiholomorphic factor), and hence vanishes. The last expression contains the Schwarzian derivative

$$\{z, w\} = \frac{2(\partial_w^3 z)(\partial_w z) - 3(\partial_w^2 z)^2}{2(\partial_w z)^2} \quad (13)$$

A similar formula is true for the antiholomorphic stress tensor $\bar{T}(\bar{w})$.

For the operator $O(w, \bar{w}) =: T(w)\bar{T}(\bar{w})$, by using a combination of the above techniques, we get a generalization of the formula (11):

$$\langle : T(w)\bar{T}(\bar{w}) : \rangle_{\text{rect}} = \left(\frac{\partial z}{\partial w} \right)^2 \left(\frac{\partial \bar{z}}{\partial \bar{w}} \right)^2 \langle T(z)\bar{T}(\bar{z}) \rangle_{\mathbb{C}} + \left| \frac{c}{12} \{z, w\} \right|^2 \quad (14)$$

2.2.1 Analytic continuation to real time correlators

As discussed before, the time-dependent wavefunction (2), or equivalently the time-dependent Heisenberg operators $O(x, t)$ can be realized by analytically continuing τ to imaginary values $\tau = it$. Thus, $O(w, \bar{w}) = O(x, \tau)$ can be interpreted as the time-dependent operator $O(x, it)$. In terms of the coordinates on the rectangle, the analytic continuation reads¹¹

$$\{w, \bar{w}\} = x \pm i\tau \xrightarrow{\tau=it} x \mp t \equiv x^\pm \quad (15)$$

This ‘Wick rotates’ the Euclidean rectangle to the Lorentzian geometry,

$$M_L = \mathbb{I} \times \mathbb{R} \ni x_\pm = x \mp t, \quad x \in \mathbb{I} = [-L/2, L/2], t \in \mathbb{R} \quad (16)$$

Note that such an analytic continuation is possible since the Euclidean observables are separately analytic in (z, \bar{z}) , and hence in (w, \bar{w}) . We will use this rule below to explicitly compute the time-dependence of one-point functions and later on, the single interval entanglement entropy.

We note here that although for these applications, we do not need to have an analytic continuation of the complex z, \bar{z} plane, we will indeed find an analytic continuation of the Euclidean map (6), *viz.* (55), from the the above geometry M_L to the Lorentzian \mathbb{R}^2 . The above map is many-to-one and one can choose a fundamental domain of the map to be a diamond-shaped region $\mathbb{D} : \{x_\pm \in (-L/2, L/2)\} \subset M_L$ in Section 4 to build a bulk

¹¹Note the convention $x^\pm \equiv x \mp t$.

geometry dual to a CFT on M_L . It has been suggested in [27], and further elaborated in [31], that thermalization appears to happen when one confines to this diamond (which is natural from the viewpoint of the \mathbb{R}^2 , whereas the actual spacetime is all of M_L , with its built-in recurrence. In Section 4, the map (55) is crucially used to construct a dual geometry for the CFT state. We will discuss this map in detail in Appendix A.2.

2.3 Behavior of the Energy density

In Euclidean CFT, the energy density is given by

$$\mathcal{E}_{Eucl}(w, \bar{w}) = \langle T_{\tau\tau} \rangle = -(\langle T(w) \rangle + \langle \bar{T}(\bar{w}) \rangle) = \frac{c}{12} (\{z, w\} + \{\bar{z}, \bar{w}\}) \quad (17)$$

where in the last step we have used (12) and its antiholomorphic counterpart. In the limits of high and low temperature, (8) and (9) respectively, the Schwarzian derivative is easy to compute, leading to the constant values

$$\mathcal{E}_{Eucl} = \begin{cases} -c\pi^2/3\beta^2, & \beta \ll L \\ +c\pi^2/12L^2, & \beta \gg L \end{cases} \quad (18)$$

Using the methods of Section 2.2.1 and the analytic continuation(15), the energy density in the Lorentzian theory is,

$$\mathcal{E}(x, t) = \langle T_{++}(x_+) + T_{--}(x_-) \rangle = \langle T_{tt} \rangle = -\langle T_{\tau\tau} \rangle = -\mathcal{E}_{Eucl}(w = x_+, \bar{w} = x_-) \quad (19)$$

Now, the high and low temperature limits are,

$$\mathcal{E}(x, t) = +c\pi^2/3\beta^2, \quad \beta \ll L \quad (20)$$

$$= -c\pi^2/12L^2, \quad \beta \gg L. \quad (21)$$

which can be identified with the well-known expressions for the thermal energy and Casimir energy respectively.

We note here that some of the results in this subsection have been obtained and discussed in [9, 27]; we include these here for the sake of completeness.

2.3.1 Time-dependence

Away from the above two limits, the energy density (19) is both space and time-dependent. We display the behaviour of the ‘normalized’ dimensionless quantity

$$\tilde{\mathcal{E}} = \frac{\mathcal{E}L^2}{c} \quad (22)$$

in Figures 2 and 3. In Figure 2, one can clearly see two crests getting reflected back and forth periodically at the boundary walls. These correspond to the holomorphic and antiholomorphic stress tensors respectively.

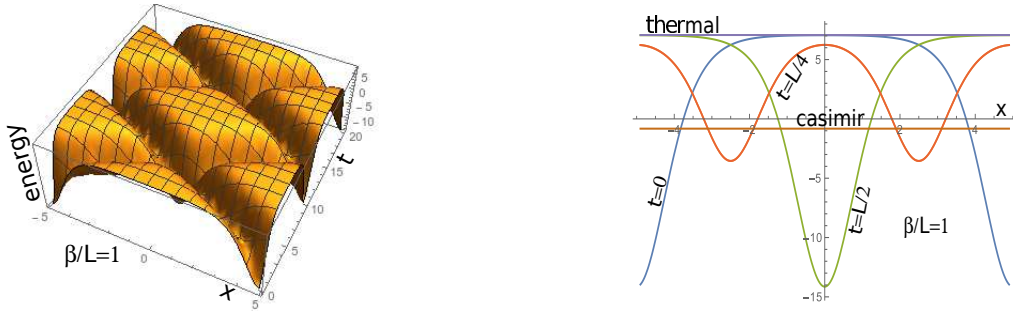


Figure 2: The time evolution of the normalized energy density $\tilde{\mathcal{E}}$ (Eq. (22)) in the quench geometry. In both the figures we have chosen $\beta = L = 10$. Left panel: The time range is taken to be $t \in [0, 2L]$. Note that there are two crests, one moving initially to the right (corresponding to $T_{++}(x_+)$ of (19)), and the other moving to the left (corresponding to $T_{--}(x_-)$). Both are reflected at the wall at $t = (n + 1/2)L, n \in \mathbb{Z}$. Right panel: Here we display, in a 2D plot, some of the features of the 3D plot at $t = 0, L/4, L/2$. At $t = 0$ there is a single local thermal region in the middle. As time progresses, it splits into two separate regions (see the curve for $t = L/4$), reaching the two ends at $t = L/2$. After this time, the two regions turn back and merge at $t = L$, as is clear from the 3D plot on the left.

2.3.2 Space dependence: Localized thermal region

In Figure 3, we plot the energy density at a fixed time $t = 0$ as a function of x for various values of the ratio β/L , with temperature increasing from left to right. In the figure, we see that for temperatures $T \lesssim 1/L$, the energy density profile has a localized region in the middle where it agrees with the thermal density. In Section 4, we will provide a holographic interpretation of this observation.

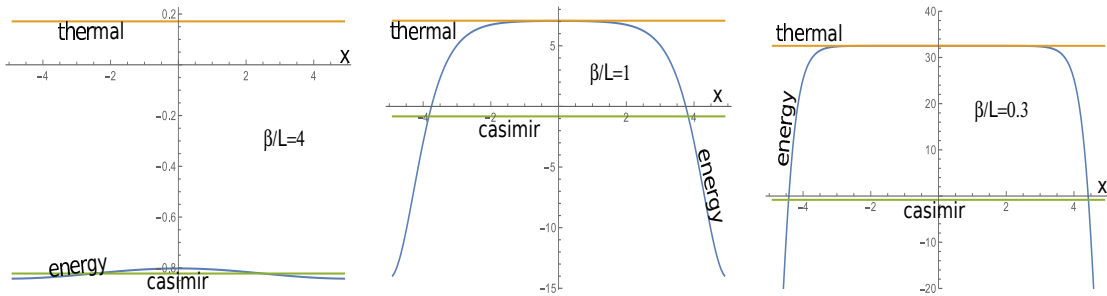


Figure 3: Plot of the normalized energy density $\tilde{\mathcal{E}}(x, t)$ at $t = 0$ for various values of $\frac{\beta}{L} = 4, 2, 0.3$. Left: $\frac{\beta}{L} = 4$. This can be interpreted as low temperature or small ‘box size’ L . The energy density approaches the uniform limiting value, the Casimir energy density computed in (21) in the low temperature limit $\frac{\beta}{L} = \infty$. Middle: $\frac{\beta}{L} = 2$. The energy density approaches the thermal value in a small region near the middle. Right: $\frac{\beta}{L} = \frac{1}{4}$. This can be interpreted as a high temperature or large box size L . The energy density matches in a large region the uniform thermal energy density computed in (20) in the limit $\frac{\beta}{L} = 0$. In the first panel, the one-point functions actually have a periodicity with a period $2L$ (see Section 4.2.1).

2.4 Thermalization and ‘revival’ of a local operator

In this section, we discuss some features of time and position dependence of one-point functions, using the formulae derived in Section 2.2. We consider primary operators of the form $O_{h,\bar{h}}(x,t)$ whose one-point functions are given by (11) with $\tau = it$. We also consider a particular quasiprimary operator $T\bar{T}(x,t)$, whose one-point function is given by (14). The results are presented in Figure 4. An important feature of the time-dependence of these operators, for a given x (see the left panel of Figure 4), is that there is a time window, $t_1 < t < t_2$, in which all these local operators ‘thermalize’, i.e., they approach their ‘thermal’ values:

$$\langle O(x,t) \rangle \rightarrow \langle O(x) \rangle_\beta + a \exp[-\gamma(t - t_1)] \quad (23)$$

In case of primary operators the thermal average $\langle O(x) \rangle_\beta$ vanishes, whereas for $T\bar{T}$, it is non-zero. It can be seen that the thermalization rate γ is given by

$$\gamma = 2\pi\Delta/\beta, \quad \Delta = h + \bar{h} = 2h \quad (24)$$

As t exceeds t_2 (which is of order $L/2$ for the operator $T\bar{T}$), the one-point function starts deviating from the thermal value and eventually goes back to its original value at $t = nL$ for some integer n (this is to be compared with the periodic behaviour termed as ‘revival’ in [9]).

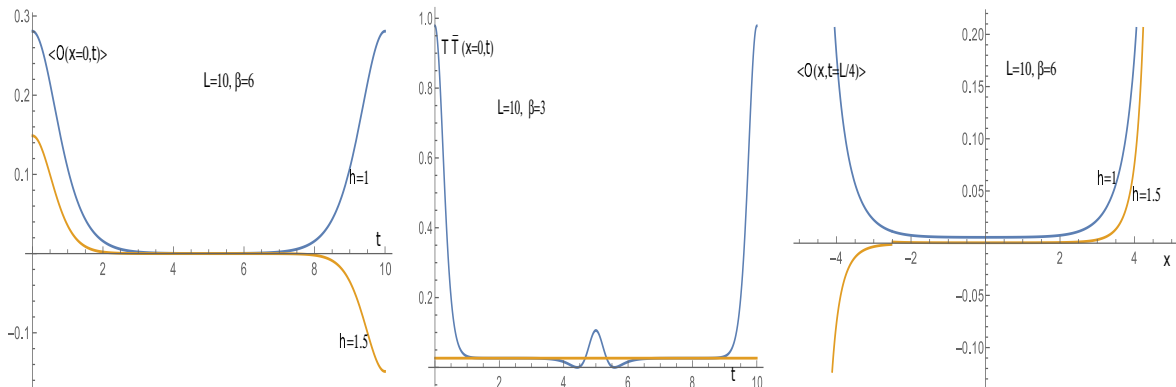


Figure 4: Plot of one-point functions as a function of x and t . The left panel shows the time-dependence of one-point functions of two primary fields $\langle O(x,t) \rangle$ with $h = \bar{h} = 1$ (blue), and $h = \bar{h} = 3/2$ (orange) at a fixed spatial position $x = 0$ (see (11)). The right panel shows the x -dependence of the same operators at a fixed $t = L/4$, which displays a homogeneous intermediate region. The middle panel shows $\langle T\bar{T} : (x,t) \rangle$ at $x = 0$ as a function of t (see (14)). The left and middle panels show the exponential decay at intermediate times to the thermal value and the eventual revival, at $t = L/2$ [9]. In the left panel the thermal value is zero. In the middle panel, the horizontal (orange) line represents the thermal value, which is non-zero since $T\bar{T}$ is a quasiprimary operator. More generally, arbitrary one-point functions show a time periodicity of $2L$ (see the derivation in Section 4.2.1).

3 Evolution of entanglement entropy following a quench

In this section we would like to compute the time-evolution of entanglement entropy (EE) of a single interval in a CFT with boundaries, following a quantum quench (as described in Section 2). We will follow up the CFT calculation in this section by a holographic computation in Section 4, and a computation using a quasiparticle picture in Section 5.

Let us consider a 2D CFT, defined by the wavefunction (1) representing a quantum quench. As explained in Section 2, the norm of the wavefunction (2), evolved over Euclidean time $\tau = \beta/4$ ¹², is given by a functional integral over a Euclidean rectangle Σ . Let us define the reduced density matrix for a spatial interval $A = \{-l/2, l/2\}$ by

$$\rho_A = \frac{1}{\sqrt{Z}} \text{tr}_{A^c} |\psi_0\rangle\langle\psi_0|, \quad \text{tr}(\rho_A) = 1 \quad (25)$$

where Z is a normalization factor. The EE for this interval is then defined as

$$S_A = -\text{tr}\rho_A \ln \rho_A \quad (26)$$

A standard procedure to compute this quantity, called the replica trick, is to first calculate the Renyi entropy

$$S_A^{(n)} \equiv \frac{1}{1-n} \text{tr}(\rho_A^n) \quad (27)$$

and then take the limit (after analytically continuing n to real values).

$$S_A = \lim_{n \rightarrow 1} S_A^{(n)} = -\left. \frac{\partial}{\partial n} \right|_{n=1} \text{tr}\rho_A^n \quad (28)$$

Computing (27) involves evaluating the partition function on the manifold Σ_n , which is an n -fold cover of the rectangle Σ branched over A . As shown in [7], this amounts to computing a two-point function, on the rectangle, of the so called n th order twist and anti-twist operators, $\sigma_+(w, \bar{w})$ and $\sigma_-(w, \bar{w})$ respectively, each with a conformal dimension $h_n = \bar{h}_n = \frac{1}{2}\Delta_n = \frac{c}{24}(n - \frac{1}{n})$. Thus,

$$\text{tr}\rho_A^n = \langle \sigma_+(w_1, \bar{w}_1) \sigma_-(w_2, \bar{w}_2) \rangle_{\text{rect}}. \quad (29)$$

where $(w_i, \bar{w}_i), i = 1, 2$ are the complex coordinates (15) of the end-points of the interval A . Let us choose the position of the end-points of the interval at a Lorentzian time t to be,

$$w_1 = -\frac{l}{2} - t, \quad \bar{w}_1 = -\frac{l}{2} + t, \quad w_2 = \frac{l}{2} - t, \quad \bar{w}_2 = \frac{l}{2} + t \quad (30)$$

¹²Quantities depending on real time are obtained by continuing to $\tau = \beta/4 + it$.

This 2-point function is obtained by pulling back a corresponding 2-point function on the upper half plane by the conformal maps (105), (87), in a generalization of Section 2.2. Hence,

$$\mathrm{tr} \rho_A^n = \prod_{i=1}^2 \left(\frac{dz_i}{dw_i} \right)^{h_n} \left(\frac{d\bar{z}_i}{d\bar{w}_i} \right)^{\bar{h}_n} \langle \sigma_+(z_1, \bar{z}_1) \sigma_-(z_2, \bar{z}_2) \rangle_{\mathrm{UHP}} \quad (31)$$

To evaluate such a 2-point function on the UHP one needs to use the method of images. However, there are subtleties associated with this method which limits its range of validity. We shall point them out in the next section before we proceed to calculate the above 2 point function using the method.

3.1 Method of Images

In [46], Cardy showed that an n -point function on the UHP satisfies the same differential equation (corresponding to a Ward Identity) as a $2n$ -point function of purely holomorphic operators on the full complex plane \mathbb{C} . The two-point function $\langle \sigma_+(z_1, \bar{z}_1) \sigma_-(z_2, \bar{z}_2) \rangle_{\mathrm{UHP}}$ is thus *related*, in this sense, to the 4-point function

$$\langle \sigma_+(z_1) \sigma_-(\bar{z}_1) \sigma_-(z_2) \sigma_+(\bar{z}_2) \rangle_C = \left(\frac{(z_1 - \bar{z}_2)(z_2 - \bar{z}_1)}{(z_1 - z_2)(\bar{z}_1 - \bar{z}_2)(z_1 - \bar{z}_1)(z_2 - \bar{z}_2)} \right)^{\Delta_n} F(\eta), \quad (32)$$

where function $F(\eta)$ is a (non-universal) function of the cross ratio

$$\eta = \frac{(z_1 - \bar{z}_1)(z_2 - \bar{z}_2)}{(z_1 - \bar{z}_2)(z_2 - \bar{z}_1)} \quad (33)$$

The relation mentioned above does not imply, however, that the two-point function on the UHP is always *equal* to the 4-point function on the plane, since, for one thing, the UHP correlator involves information about the boundary condition on the boundary of the UHP whereas the planar correlator does not involve any such information¹³.

Having said this, it turns out that there are certain limits where the two correlators are, in fact, essentially¹⁴ equal. One of them is the high temperature limit where both the 2 and the 4-point functions factorize in one way or the other. In such a case, the UHP correlator does turn out to be essentially independent of the boundary state. For intermediate temperatures, however, there is no such factorization and the two-point function on the UHP is different from the 4-point function on \mathbb{C} due to the presence of the boundary.

There is another limit, as we will study, in which the equality holds (in fact, at all temperatures this time). This is the large central charge limit. As we shall see in Section 3.4, in this limit, the four point function is easily evaluated and becomes essentially equal to the two-point function on the UHP. Here too the information about the boundary condition is lost in the large c limit.

¹³We thank Justin David and Tadashi Takayanagi for crucial discussions on this issue.

¹⁴In this subsection, we use the word “essentially” to mean up to an irrelevant proportionality constant.

3.2 Large L/β limit

In the limit of large system size L ¹⁵, the conformal map is given by (8). The computation of EE described above reduces, in this limit, to the analysis of [8, 14]. The complex coordinates (30) are mapped to

$$z_1 = ie^{-\frac{2\pi}{\beta}(-\frac{l}{2}-t)}, \bar{z}_1 = -ie^{-\frac{2\pi}{\beta}(-\frac{l}{2}+t)}, z_2 = ie^{-\frac{2\pi}{\beta}(\frac{l}{2}-t)}, \bar{z}_2 = -ie^{-\frac{2\pi}{\beta}(\frac{l}{2}+t)} \quad (34)$$

on the upper half plane. Here we have assumed that $t/l \ll L$. Therefore, the cross ratio η in (33) becomes

$$\eta = \frac{2 \cosh^2 \frac{2\pi t}{\beta}}{\cosh \frac{2\pi l}{\beta} + \cosh \frac{4\pi t}{\beta}} \quad (35)$$

When $t/\beta, l/\beta \gg 1$, the cross ratio behaves as

$$\eta \simeq \frac{e^{\frac{4\pi t}{\beta}}}{e^{\frac{4\pi t}{\beta}} + e^{\frac{2\pi l}{\beta}}} \quad (36)$$

It is easy to verify that,

$$\eta \rightarrow \begin{cases} 0 & \text{for } t < l/2 \\ 1 & \text{for } t > l/2 \end{cases} \quad (37)$$

where we have assumed $|t - l/2| \gg \beta$. Both the limits of η correspond to a factorization of the four-point function (32) into a product of two-point functions in the two crossed channels, respectively. This leads to a simpler calculation of the EE which gives

$$S_A = \begin{cases} \frac{2c\pi t}{3\beta} & \text{for } t < l/2 \\ \frac{c\pi l}{3\beta} & \text{for } t > l/2 \end{cases} \quad (38)$$

where a divergent constant has been subtracted [8].

These results are universal since they depend only on the central charge of the CFT. The behaviour (38) represents the linear rise of the EE followed by the saturation to the thermal value (see Figure 6, left part of the third panel). By the periodicity properties mentioned in Section 4.2.1, we can also show that CFT results reproduce the right part of the third panel of Figure 6. One way to see this is to note that for $L - t, l \ll L$ the map (6) reduces to a map similar to (34), with $t \rightarrow L - t$.

¹⁵Defined in the sense of the limit (a) of footnote 25.

3.3 Low temperature (L/β small)

In the low temperature limit¹⁶, the conformal map is given by (9). Using this, the w -coordinates (30) are mapped to

$$\begin{aligned} z_1 &= i \cot \left(\frac{\pi}{4} + \frac{\pi(-l/2 - t)}{2L} \right), & \bar{z}_1 &= -i \cot \left(\frac{\pi}{4} + \frac{\pi(-l/2 + t)}{2L} \right) \\ z_2 &= i \cot \left(\frac{\pi}{4} + \frac{\pi(l/2 - t)}{2L} \right), & \bar{z}_2 &= -i \cot \left(\frac{\pi}{4} + \frac{\pi(l/2 + t)}{2L} \right). \end{aligned} \quad (39)$$

The cross-ratio (33) now becomes

$$\eta = \cos^2 \frac{\pi l}{2L} \quad (40)$$

Thus, unlike in the high temperature limit, the cross ratio does not take a special value. Depending on the size of the interval l , it can lie anywhere between 0 and 1. Consequently, the four-point function (32) does not factorize into two-point functions. This implies that the CFT EE remains a non-universal quantity, depending on the particular CFT under consideration.

A puzzle The above remark immediately raises the following puzzle. We will see in Section 4.1, the holographic EE, as computed using (61) and (66), is independent of the details of the dual CFT (except for the dependence on the central charge c which determines the Newton's constant through (60)).¹⁷

The puzzle is that while the holographic EE is universal, the CFT EE certainly does not appear to be so. How does one reconcile this with AdS/CFT? Also, what is the CFT calculation which will agree with the hEE at all temperatures and exhibit universality?

Resolution This puzzle will be resolved in the next subsection, by appealing to the *large central charge* limit.

3.4 Universality of the Entanglement Entropy at large central charge

3.4.1 At Low Temperature

One way of obtaining universal results for the EE, (as will be shown in the low temperature bulk calculations), from the CFT, is by looking at the large c systematics (similar issues

¹⁶Defined in the sense of limit (c) of footnote 25.

¹⁷This is a recurrent theme in AdS/CFT. A similar observation is: many different CFT states appear to evolve into states described by black holes. The emergence of universality in the bulk in that context is related to the universality of thermal physics.

have been addressed in [42]). As has been mentioned, the calculation of $\text{tr}\rho_A^n$ on the manifold Σ_n , can be mapped to the calculation of the two point correlator of n-th order twist and anti-twist operators on the UHP. Using the method of images, this is equivalent to a four point function of two twist and two anti-twist operators on \mathbb{C} . The four point function is then,

$$\text{tr}\rho_A^n = \prod_{i=1}^2 \left(\frac{dz_i}{dw_i} \right)^{h_n} \left(\frac{d\bar{z}_i}{d\bar{w}_i} \right)^{\bar{h}_n} \mathcal{G}_4, \quad \mathcal{G}_4 \equiv \langle \sigma_+(z_1)\sigma_-(\bar{z}_1)\sigma_+(\bar{z}_2)\sigma_-(z_2) \rangle_{\mathbb{C}}$$

For convenience, we send the four points $(z_1, \bar{z}_1, z_2, \bar{z}_2)$ to $(\infty, 1, 0, \eta)$, such that

$$\mathcal{G}_4 = (z_{1\bar{2}}z_{\bar{1}2})^{-2h_n} G_n(\eta), \quad G_n(\eta) = \langle \sigma_+(\infty)\sigma_-(1)\sigma_+(\eta)\sigma_-(0) \rangle_{\mathbb{C}} \quad (41)$$

Consider the scaled 4 point function in the $\eta \rightarrow 0$ channel. In the large central charge limit, all the conformal blocks exponentiate ([47]). The form of the function is,

$$G_n(\eta) = \sum_p a_p e^{-\frac{nc}{8} f_p(h_n, \eta; nc)} \quad (42)$$

Recent results ([40]) suggest that it is only the vacuum block that dominates the above sum over intermediate operators. In that case, the 4-point function is,

$$G_n(\eta) \approx e^{-\frac{nc}{8} f_0(h_n, \eta; nc)} \quad (43)$$

Taking the four points $z_{1,2}, \bar{z}_{1,2}$ to be given by (39), we get the cross-ratio to be,

$$\eta = \frac{z_{1\bar{1}}z_{2\bar{2}}}{z_{1\bar{2}}z_{2\bar{1}}} = \cos^2 \frac{\pi l}{2L} \quad (44)$$

From ([40]), one knows that the result for the vacuum block (in the $\eta \rightarrow 0$ channel) is,

$$f_0(h_n, \eta; nc) = 12\alpha \log(\eta) + \mathcal{O}(\alpha^2) \quad (45)$$

where $\alpha = \frac{1}{12}(n-1)(=h_n/c)$. Hartman's result tells us that we can extrapolate the result found around $\eta = 0$ up till $\eta = \frac{1}{2}$ owing to monotonicity of the conformal blocks as a function of η for light operator exchanges. A similar statement holds in the other channel around $\eta = 1$. The vacuum block in that case is,

$$f_0(h_n, \eta; nc) = 12\alpha \log(1-\eta) + \mathcal{O}(\alpha^2) \quad (46)$$

Here, again, the results can again be extrapolated up to $\eta = \frac{1}{2}$. This enables us to state that the purely holomorphic Euclidean 4-point function is in fact equal to the 2-point function on the UHP. Again, the interesting thing to notice is that the information about the boundary gets completely lost in this equivalence at large c !

The Entanglement Entropy in the s-channel ($\eta \rightarrow 0$) is then,

$$S_A = \lim_{n \rightarrow 1} \frac{1}{1-n} \log \text{Tr} \rho_A^n = \lim_{n \rightarrow 1} \left[\frac{4h_n}{1-n} \log\left(\frac{\pi}{2L}\right) - \frac{nc}{6} \frac{1}{1-n} 12\alpha \log(\eta) \right] \quad (47)$$

where the first term comes from the Jacobian and the prefactor in 41. With $\alpha = h_n/c$ and $\eta = \cos^2(\frac{\pi l}{2L})$, we get,

$$S_A = \frac{c}{3} \log \left(\frac{2L}{\pi a} \cos \frac{\pi l}{2L} \right) \quad (48)$$

This result is, of course, valid up to $\eta = 1/2$ and hence, for $L/2 \leq l < L$. In the other channel $\eta \rightarrow 1$,

$$S_A = \frac{c}{3} \log \left(\frac{2L}{\pi a} \sin \frac{\pi l}{2L} \right) \quad (49)$$

This is valid for $0 \leq l \leq L/2$. In both the above cases, we have introduced the UV cut-off a by hand to regulate the answers. As, we will see later, these answers match exactly with the holographic results in the low-temperature limit.

3.4.2 For All Temperatures

The results obtained at low temperatures for large c are much more general. In fact, we would like to show the equivalence of these results with the lengths of the bulk geodesics, which can be calculated for all temperatures. The analysis of the four point function on \mathbb{C} is completely general. The information about the initial nature of the geometry (a rectangle in this case), is contained in the pull-back maps and hence in the Jacobian factors. Only the cross-ratio on the plane knows about the initial geometry through the pull back maps. Let us calculate the entanglement entropy on the plane and use an unspecified conformal transformation to pull it back onto a non-trivial geometry.

On the plane,

$$\text{tr} \rho_A^n = \prod_{i=1}^2 \left(\frac{dz_i}{dw_i} \right)^{h_n} \left(\frac{d\bar{z}_i}{d\bar{w}_i} \right)^{\bar{h}_n} \mathcal{G}_4 \quad (50)$$

Let us call the Jacobian factors $J = \prod_{i=1}^2 \left(\frac{dz_i}{dw_i} \right) \left(\frac{d\bar{z}_i}{d\bar{w}_i} \right)$ for simplicity. Then (as we saw in the previous section), for the $\eta \rightarrow 1$ channel,

$$\begin{aligned} S_A &= \lim_{n \rightarrow 1} \frac{1}{1-n} \left[h_n \log \left(\frac{a^4 J}{(z_{1\bar{2}} z_{\bar{1}2})^2} \right) - \frac{nc}{6} 12\alpha \log(\eta) \right] \\ &= \lim_{n \rightarrow 1} \frac{2h_n}{n-1} \left[\log \left(\frac{z_{1\bar{2}} z_{\bar{1}2}}{a^2 \sqrt{J}} \right) + n \log(\eta) \right] \\ &= \frac{c}{6} \log \left(\frac{\eta}{a^2} \frac{z_{1\bar{2}} z_{\bar{1}2}}{\sqrt{J}} \right) \end{aligned} \quad (51)$$

Note, the factor of a^4 in the first line of the expression has been introduced for dimensional reasons and has a length dimension. With the identifications, $c = \frac{3}{2G_3}$ and $\eta = \frac{z_{1\bar{1}}z_{2\bar{2}}}{z_{1\bar{2}}z_{2\bar{1}}}$, the above EE is,

$$S_A = \frac{1}{4G_3} \log \left(\frac{z_{1\bar{1}}z_{2\bar{2}}}{a^2\sqrt{J}} \right) \quad (52)$$

This expression for the entanglement entropy exactly coincides the sum of the bulk geodesic lengths between the boundary points (z_1, \bar{z}_1) and (z_2, \bar{z}_2) (with the identifications $z_{\pm} = f(x_{\pm})$), in the geometry corresponding to the pulled back (non-trivial) surface, at all temperatures. This is the ‘disconnected’ channel in (66).

Similarly, when $\eta \rightarrow 0$, we shall have to use the conformal block in the other channel. Now, $(1 - \eta) = \frac{z_{12}z_{\bar{1}\bar{2}}}{z_{1\bar{2}}z_{2\bar{1}}}$. Using this, the entanglement entropy is,

$$\begin{aligned} S_A &= \lim_{n \rightarrow 1} \frac{1}{1-n} \left[h_n \log \left(\frac{a^4 J}{(z_{12}z_{\bar{1}\bar{2}})^2} \right) - \frac{nc}{6} 12\alpha \log(1 - \eta) \right] \\ &= \frac{c}{6} \log \left(\frac{(1 - \eta) z_{12}z_{\bar{1}\bar{2}}}{a^2 \sqrt{J}} \right) \\ &= \frac{1}{4G_3} \log \left(\frac{z_{12}z_{\bar{1}\bar{2}}}{a^2\sqrt{J}} \right) \end{aligned} \quad (53)$$

This matches with the bulk entropy in the ‘connected’ channel in (66) with geodesics joining the points (z_1, z_2) and (\bar{z}_1, \bar{z}_2) .

4 Bulk dual

In this section we discuss a holographic dual to the above two dimensional quenches [17]. It is known that a class of two dimensional CFTs with a large central charge c have an equivalent description in terms of gravity in three dimensional anti de Sitter space (AdS_3). In Poincaré coordinates the metric of AdS_3 is given by

$$ds^2 = \frac{d\zeta^2 + dz_+ dz_-}{\zeta^2}. \quad (54)$$

Here $\zeta = 0$ is the conformal boundary of AdS_3 . The boundary coordinates $z_{\pm} = z_1 \mp z_0$ describe the plane where the dual (Lorentzian) CFT lives. We will also consider the Euclidean continuation of the above metric where we will set $z_{\pm} = \mp i\{z, \bar{z}\}$ (see (101), Appendix A.2). The corresponding dual CFT on the complex z -plane will then be Euclidean.

A holographic description of the CFT on a space with boundaries (BCFT) has been proposed in [34, 35, 36, 37, 38]. According to this proposal, the holographic dual of the BCFT on the upper half plane $\{(z_1, z_0) | z_0 > 0\}$ is given by the $z_0 > 0$ region of the Poincaré

AdS_3 . The $z_0 = 0$ plane serves as a boundary of the holographic spacetime¹⁸, with the boundary condition that the extrinsic curvature of the boundary vanishes $K_{\mu\nu} = 0$ ¹⁹, and ends (at $\zeta = 0$) on the boundary of the UHP. A schematic picture is presented in Figure 5.

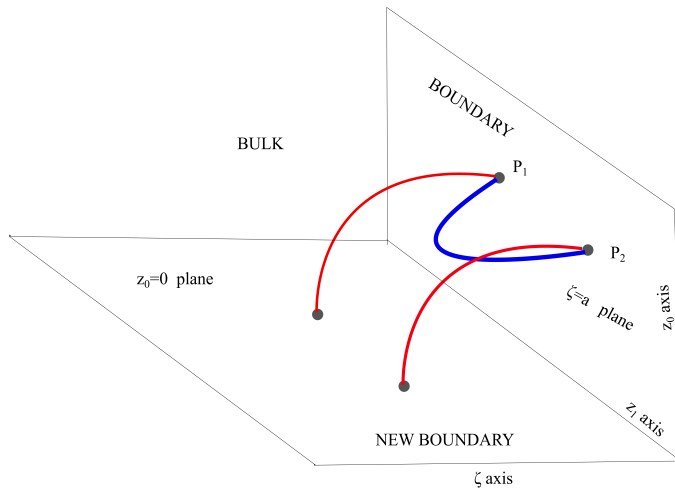


Figure 5: Holographic dual to BCFT on the UHP (upper half plane). A one-point function in the UHP is given by an extremal geodesic emanating from the relevant boundary point and ending on the boundary plane (the length of this is half of the geodesic connecting the boundary point and its image). Entanglement entropy of the interval connecting two boundary points P_1 and P_2 is given by the minimum (64) of the length of extremal geodesics connecting these points and their images pairwise. We call the ‘blue’ and ‘red’ configurations the ‘connected’ and ‘disconnected’ channels respectively.

The above description gives the bulk dual of a Lorentzian CFT on the UHP; we would, however, like to obtain the bulk dual for a CFT on a manifold (16), $M_L = \text{interval} \times \mathbb{R}$. Now, in Appendix A.2 we will find a map from the manifold M_L to the UHP, given by (102):

$$z_{\pm} = f_{\pm}(x_{\pm}), \quad f_+(x) = f_-(x) = f(x) \equiv -b \frac{\text{sn} \left[\frac{4K(b^4)}{\beta}(x - L/2), 1 - b^4 \right]}{\text{cn} \left[\frac{4K(b^4)}{\beta}(x - L/2), 1 - b^4 \right]} \quad (55)$$

Bulk dual through large diffeomorphisms Our strategy to find a bulk dual to the CFT on M_L will be to find a solution to Einstein’s equations with a negative cosmological constant whose boundary is M_L . This problem can be solved by the method introduced in [39], where it was shown (building on the works of [49] and [50]) how solutions diffeomorphic to the AdS_3 geometry (54) (which are hence solutions to Einstein equations) can be found

¹⁸In a recent proposal [48] a stress-tensor has been ascribed to this plane as in the case of a D-brane.

¹⁹This boundary condition has a one parameter generalization [36, 37] which corresponds to available boundary conditions in the BCFT.

where the diffeomorphism is non-trivial at the boundary and reduce to the map (55). The diffeomorphisms alluded to here are analogous to ‘large gauge transformations’ [51, 52] and are called ‘large’ diffeomorphisms or ‘solution generating diffeomorphisms’ [18]. Of course, large diffeomorphisms which reduce to a specific conformal transformation f_{\pm} are not unique since one can always compose with any local diffeomorphism which reduces to identity at the boundary. This ambiguity can be removed, however, if one demands that the resulting bulk metric is in the Fefferman-Graham gauge. These ideas have been used in the study of quantum quenches in [17, 18, 39]. The quantitative form of ‘large’ diffeomorphism was found by ([39]) and is given by

$$\zeta = 4z \frac{(f'_+ f'_-)^{3/2}}{D}, \quad z_{\pm} = f_{\pm}(x_{\pm}) - \frac{2z^2 f'_{\pm}{}^2 f''_{\mp}}{D}, \quad D = 4f'_+ f'_- + z^2 f''_+ f''_- \quad (56)$$

Note, as a check, that as $\zeta \rightarrow 0$ (the boundary of the Poincaré metric (54)), we have $z \rightarrow 0$ (assuming that D remains finite), and $z_{\pm} \rightarrow f_{\pm}(x_{\pm})$. It is important to note that for functions $f_{\pm}(x_{\pm})$ which are not one-to-one and have vanishing Jacobians at the boundaries of fundamental domains, one must restrict the above transformation (56) to a given choice of fundamental domain.

Applying this large diffeomorphism to the Poincaré metric, we get the following metric [50]

$$ds^2 = \frac{dz^2}{z^2} + \frac{1}{4} (L_+ dx_+^2 + L_- dx_-^2) + \left(\frac{1}{z^2} + \frac{z^2}{16} L_+ L_- \right) dx_+ dx_- \quad (57)$$

where L_{\pm} are given in terms of Schwarzian derivatives (13) of the boundary conformal map

$$L_{\pm} = -2\{z_{\pm}, x_{\pm}\} = \frac{3f_{\pm}''^2 - 2f'_{\pm} f_{\pm}'''}{f_{\pm}'^2} \quad (58)$$

The metric ((57)) is called the Fefferman-Graham metric and has been written in the Fefferman-Graham gauge. Note that as $z \rightarrow 0$, the leading terms of this metric reduce to that of the Poincaré metric (54). The two metrics, however, represent physically different solutions of the theory due to the existence of the subleading terms of the metric (57) involving the L_{\pm} terms which represent nontrivial stress tensors at the boundary [53]. These L_{\pm} 's capture the ‘surface charges’ of [49] characterizing the quantum state. The precise relation ([50],[53]) between L_{\pm} and the CFT stress tensors is,

$$T_{\pm,\pm}(x_{\pm}) = \frac{L_{\pm}}{16G_3} = \frac{c}{24} L_{\pm} \quad (59)$$

where we have used the following relation between the central charge of the CFT and the 3D Newton’s constant

$$c = \frac{3}{2G_3}. \quad (60)$$

Properties of the metric: The metric (57), therefore, provides the promised solution to the Einstein's equations (with $\Lambda < 0$) whose conformal boundary coincides with the manifold M_L . Hence, gravity on this metric provides the geometric dual to the CFT on M_L (which is the CFT of our interest).

We have shown in Appendix C the high temperature limits and low temperature limits of the geometry (57) represent the BTZ black hole and the global AdS respectively. We can show that at sufficiently high temperatures the geometry contains a horizon. For the purposes of the rest of the paper, the important property of the metric (56) is that the spatial direction x is compactified with a periodicity L (i.e. equal to the spatial size L). This follows as a consequence of the periodicity properties of the Elliptic functions (see, e.g. (91) and similar statements for the Lorentzian map).

The periodicity properties of the CFT observables can be holographically interpreted in terms of the above periodicity property of the bulk metric. Thus, e.g. a two-point function, which can be specified by the geometric properties of a geodesic with end-points at the boundary, are periodic because the geodesic will come back to itself after a time period L . We will find below an explicit example of how this happens in case of the holographic EE.

Other candidate bulk duals It is important to note that in related contexts, somewhat different proposals for bulk dual geometries have appeared. For example, the bulk dual to the large L limit of the CFT studied here, used by [14] is obtained by first dividing the Penrose diagram of an eternal BTZ black string geometry vertically by an end-of-the world brane and then taking the top half of it as the relevant bulk dual geometry. We are currently investigating the relation between our proposal and this geometry. The hEE computed in both geometries turn out to be the same. Some other proposals for bulk geometries dual to quantum quench involve the AdS-Vaidya metric, see, e.g. [6].

4.1 Holographic quantum quench and entanglement entropy

As mentioned in Section 4, for a class of 2D CFTs with a large central charge c , a holographic description is available in terms of a weakly coupled gravity dual in asymptotically AdS₃ spaces. A computation of the CFT partition function over the branched cover Σ_n maps to a computation of the bulk partition function over a dual geometry whose conformal boundary coincides with Σ_n [40, 54, 55]. As shown in [55], this observation leads to the well-known Ryu-Takayanagi formula [56, 57] for the holographic entanglement entropy (**hEE**) of an interval A

$$S_{hol,A} = \text{ext} \frac{l(\gamma_A)}{4G_3}, \quad (61)$$

where γ_A is the extremal curve in the bulk ending at the boundary of the interval A , $l(\gamma_A)$ is the length of this curve, and G_3 is Newton's constant which is related to the central

charge c of the dual CFT by (60). The extremum is taken among all curves γ_A which are homotopic to the subsystem A .

Let us first compute (61) in the bulk dual of the BCFT on the upper half plane. The dual geometry is the upper half of the spacetime (54). Suppose that the boundary of the subsystem A consists of two points $P_1 = z_{\mu,1} = (z_{+,1}, z_{-,1}), P_2 = z_{\mu,2} = (z_{+,2}, z_{-,2}), \mu = +, -$. In this case we have two extremal *geodesics*, as shown in Figure 5:

(i) One is a geodesic connecting P_1 and P_2 , which we call the connected geodesic, whose length is

$$l(\gamma_A)_c = 2 \log \frac{|P_1 - P_2|}{\zeta_{min}} = 2 \log \frac{\sqrt{(z_{+,1} - z_{+,2})(z_{-,1} - z_{-,2})}}{\zeta_{min}}, \quad (62)$$

where ζ_{min} denotes the UV cut-off in the CFT which, by the rules of AdS/CFT, corresponds to placing the asymptotic boundary at $\zeta = \zeta_{min}$ (this regulates the extremal surface area which will diverge otherwise). $|P_1 - P_2|$ denotes the distance measured in the flat boundary metric $ds^2 = dz_+ dz_-$.

(ii) The presence of the additional spacetime boundary at $z_0 = 0$, leads to the existence of an extra geodesic consisting of two independent geodesic segments, each of which connects P_1 (or P_2) to this new boundary. We will call this the disconnected geodesic; the length of each segment, say the first one, is half of that of a geodesic connecting P_1 to each its ‘image point’ P'_1 below the boundary (similarly with P_2). Combining the two segments, we get

$$l(\gamma_A)_{dc} = \log \frac{|P_1 - P'_1|}{\zeta_{min}} + \log \frac{|P_2 - P'_2|}{\zeta_{min}} \quad (63)$$

The entanglement entropy (61) is determined by taking the minimum among these [57].

$$S_{hol,A} = \frac{1}{4G_3} \times \min\{l(\gamma(A))_c, l(\gamma_A)_{dc}\} \equiv \min\{S_c, S_{dc}\} \quad (64)$$

Fluctuation of the UV cut-off with a large diffeomorphism The construction here gives the hEE for the bulk dual of a CFT on the UHP, which is (54) with an additional boundary. As we found in Section 4, the bulk dual to the BCFT on the rectangle, which is of our original interest, is given by the geometry (57). Since the latter metric is related to the former by a diffeomorphism (which is non-trivial at the boundary), the extremal geodesics in the latter metric can be obtained by pulling back (62), (63) into the geometry. This prescription is known to reproduce the time evolution of entanglement entropy in various quantum quenches [16, 17]. The effect of the large diffeomorphism can be represented by a fluctuation of the end-points P_1, P_2 [17, 18], while the inside geometry remains identical. The effect of this is that the point P_1 , represented by the coordinates $(\zeta_{min}, z_{\pm,1})$ in the Poincare geometry (54) is transformed to $(z_{min}, x_{\pm,1})$ according to (56). We define the original CFT to be that on the rectangle, with a lattice cut-off a . In AdS/CFT, this

instructs to introduce a UV cut-off surface $z_{min} = a$ in the geometry (57). Near the horizon, using the $z \rightarrow 0$ limit of (56), we have

$$\zeta_{1,min} = a\sqrt{f'_+(x_{+,1})f'_-(x_{-,1})} \quad (65)$$

and similarly for the point P_2 . In other words, insisting on a given cut-off in the original CFT leads to a local definition of the UV cut-off, as above. The prescription for generalization of formulae like (62) to take this into account is simple [17, 18]: just replace ζ_{min} in (62) by $\sqrt{\zeta_{1,min}\zeta_{2,min}}$.

Expression for the hEE Using these ingredients we get the following formulae for the extremal length of two geodesics in the new bulk geometry (57):

$$\begin{aligned} l(\gamma_A)_c &= \log \frac{(f(x_{+,1}) - f(x_{+,2}))(f(x_{-,1}) - f(x_{-,2}))}{a^2 \sqrt{f'(x_{+,1})f'(x_{+,2})f'(x_{-,1})f'(x_{-,2})}}, \\ l(\gamma_A)_{dc} &= \log \frac{(f(x_{+,1}) - f(x_{-,1}))(f(x_{+,2}) - f(x_{-,2}))}{a^2 \sqrt{f'(x_{+,1})f'(x_{-,1})f'(x_{+,2})f'(x_{-,2})}} \end{aligned} \quad (66)$$

Here $f_+ = f_- = f$ is as defined in (55).

The boundary points of interest in this problem are given by the coordinates (which are Lorentzian versions of the points (30))

$$x_{\pm,1} = -l/2 \mp t, \quad x_{\pm,2} = l/2 \mp t \quad (67)$$

These represent the end-points of the entangling interval (region A) at time t .

4.2 Evolution of holographic entanglement entropy

In this section, we compute time evolution of holographic entanglement entropy in the global quench with boundaries, using the prescription we mentioned in the previous subsection. We mainly focus on the low temperature limit $\frac{L}{\beta} \rightarrow 0$ as well as the high temperature limit $\frac{L}{\beta} \rightarrow \infty$. We also compare the result to the naive CFT entanglement entropy derived by neglecting the function $F(z)$ in (32) which is the theory dependent part of the four point function (32). We find that whereas they do not agree in the low temperature limit, they do agree in the high temperature limit. This suggests that the behavior of the entanglement entropy, as computed from the bulk dual, is universal, which coincides with the usual universality (coming from the factorization limit) at high temperatures, but it is a *new universality* at low temperatures (see Section 3.4).

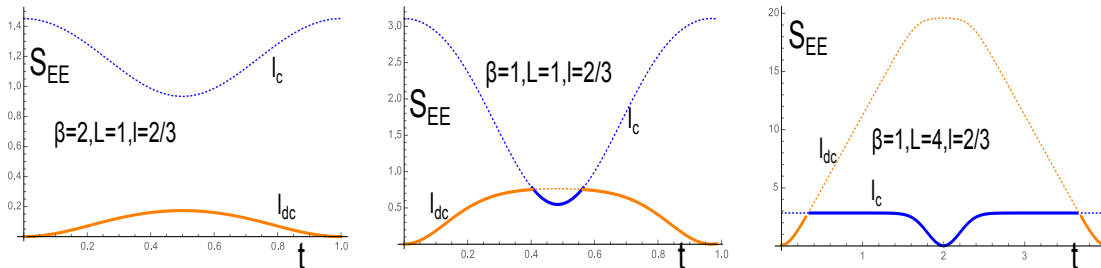


Figure 6: Plot of the time evolution of the length of geodesics which determine, via (61), (64), the entanglement entropy (S_{EE}) of an interval with end-points at $\mp l/2$ (for convenience we have rescaled the geodesic lengths by a factor of $\frac{1}{2}$ and adjusted the height of each curve by choosing the UV cut-off a in (66) appropriately). The length of the connected path, l_c (62) is shown in blue, and that of the disconnected, l_{dc} (63) is shown in red. The left panel corresponds to low temperature with $L/\beta = 1/6$, the middle panel to intermediate temperature with $L/\beta = 1$ and the right panel corresponds to large L (or high temperature²¹) with $L/\beta = 4$. By the minimum prescription of [57], (64), S_{EE} is given by the curve segments which lie lower; these are represented by solid lines in the figures. The curve segments lying higher are not relevant in the computation of EE, and are represented by dotted lines. Note the exchange of dominance (‘phase transition’) for intermediate and high temperatures. The above EE is exactly reproduced by the CFT calculations in the large c limit (see Section 3.4). For the rightmost panel, except for the central dip, the EE can be seen to match the CFT result even without the help of large c asymptotics, using factorization into appropriate two-point functions at large L/β .

4.2.1 Time periodicity of two-point functions and the hEE

Note that the map $f(x_{\pm})$ appearing in the above expressions satisfies (cf. (91)) $f(x_{\pm}) = f(x_{\pm} + 2L)$. Since the spatial locations of the boundary points are fixed as in (67), the above periodicity implies a periodicity in time $t \equiv t + 2L$ of two-point functions of operators whose AdS representation is in terms of geodesics. The periodicity here can be geometrically understood as follows. The map (56) with periodic $f_{\pm} = f$ effects a quotienting of the Poincare geometry. As time progresses, each end-point of a geodesic climbs along a straight line in the x - t plane; the light-cone coordinates both trace out a periodic path on the cylinder (which is double the manifold M_L (16)), leading to the time-periodicity mentioned above.

For the hEE of a centrally located interval (with end-points located at $x = \mp l/2$), the period, in fact, turns out to be L rather than $2L$, as in Figure 6. This periodicity holds for both the connected or the disconnected expression (l_c or l_{dc}) in (66). To see this, note that the odd (even) parity of the sn (respectively, cn) functions imply that $f(x_{\pm,1} + L) = -f(x_{\mp,2})$, $f(x_{\pm,2} + L) = -f(x_{\mp,1})$. Here we have used the definitions (67). In a similar way we can also show the symmetry $l_c(t) = l_c(L - t)$, $l_{dc}(t) = l_{dc}(L - t)$, which is evident in Figure 6.

²¹Strictly speaking, we distinguish between $L \rightarrow \infty$ and $\beta \rightarrow 0$ in the sense of footnote 25.

4.2.2 Low temperature limit $\frac{L}{\beta} \rightarrow 0$

In this limit the map f_{\pm} of (55) reduces to the analytic continuation of (9), namely

$$z_{\pm}(x_{\pm}) = \cot(\pi/4 + \pi x_{\pm}/(2L)) \quad (68)$$

By using this conformal map, and the formalism described above, we can calculate the contribution of the connected surface to the holographic entanglement entropy S_c , and the contribution of the disconnected surface S_{dc} .

$$S_c = \frac{c}{3} \log \left[\frac{2L}{a\pi} \sin \left(\frac{\pi l}{2L} \right) \right], \quad S_{dc} = \frac{c}{3} \log \left[\frac{2L}{a\pi} \cos \left(\frac{\pi l}{2L} \right) \right] \quad (69)$$

In this case the entanglement entropy does not depend on time, hence we are interested in how this depends on the size of the subsystem A . By taking the minimum between S_c and S_{dc} we get,

$$S_{hEE} = \begin{cases} \frac{c}{3} \log \left[\frac{2L}{a\pi} \sin \left(\frac{\pi l}{2L} \right) \right] & l < \frac{L}{2} \\ \frac{c}{3} \log \left[\frac{2L}{a\pi} \cos \left(\frac{\pi l}{2L} \right) \right] & l > \frac{L}{2} \end{cases} \quad (70)$$

When the size of the subsystem is smaller than the half of the subsystem $l < \frac{L}{2}$, the result is the same as that in the vacuum state on a cylinder with circumference $2L$. This is natural because the local physics is the same in both cases. When $l > \frac{L}{2}$, they become different. This is necessary because entanglement entropy has to vanish if we take the subsystem to be the total system.

Nontrivial agreement with CFT Note that the holographic EE obtained above exactly agrees with the CFT EE, discussed in Section 3.4 (see (51)). As explained before, this is a nontrivial agreement, since in general, including at low temperatures, the CFT EE is, *a priori*, non-universal, being given by a four-point function. However, as we found in Section 3.4, in an appropriate limit of large central charge, one recovers a universal result (51) which depends only on the central charge and no other feature of the CFT. This then agrees with the hEE obtained above.

4.2.3 Large L limit $\frac{L}{\beta} \rightarrow \infty$

If we slightly turn on the temperature, the area of the extremal surfaces starts to depend on time. In the low temperature regime, the area of one extremal surface (the disconnected one) is always smaller than the other one (the connected one) for a fixed subsystem size l (see Figure 6). However above some value of the temperature, there are phase transitions. When $0 < t < L/2$, it happens twice. We can check that for sufficiently large $\frac{L}{\beta}$, the area of disconnected surface is smaller at early times, but since S_{dc} linearly grows in time, the connected surface becomes the minimal surface at some critical time. This is the first phase

transition. As we will see in the next section, this critical time t_c depends on the size of the subsystem. When $l > \frac{L}{2}$, this is given by $t_c = \frac{L-l}{2}$. When $l < \frac{L}{2}$, this critical time is $t_c = \frac{l}{2}$. This is natural because if we take a small subsystem limit $\frac{l}{L} \ll 1, \frac{L}{\beta} \gg 1$, the result should approach that of the usual global quenches without boundary walls (see Figure 6). As is obvious from the periodicity mentioned in Section 4.2.1), we encounter a second phase transition after t crosses $L/2$, when the disconnected surface becomes minimal again. The central dip in this figure cannot be understood from CFT, but in the next section on quasiparticles, we have an accurate understanding of the entire plot of the third panel.

5 The quasiparticle picture of the evolution of the entanglement entropy

The evolution of the entanglement entropy at sufficiently high temperatures limit can be interpreted by the free-streaming quasiparticle picture of [8]. In this picture, one models the quenched state as populated by entangled quasiparticles pairs at every point consisting of a left- and a right-moving particle, each moving at the speed of light. The entanglement entropy of an interval A increases by $\frac{c\pi}{6\beta}$ when a quasiparticle goes outside (inside) the interval while its entangled partner is still inside (outside) the interval.

5.1 The quasiparticle interpretation for global quench for infinite spatial size

In this subsection we will review the interpretation of the time evolution of the entanglement entropy in the global quench on the non-compact line \mathbb{R} . The contribution of the quasiparticle pairs, which are located in $[-(|x|+d|x|), -|x|]$ initially, to the entanglement entropy at a fixed time, depends on the value of $|x|$. If the quasiparticles are located inside the interval, $A = \{|x| < \frac{l}{2}\}$ at the initial time, the contribution to the entanglement entropy $s_A^{(1)}(|x|, t)$ is given by

$$s_A^{(1)}(|x|, t) = \frac{c\pi}{6\beta} \left[\theta \left(t - (-|x| + \frac{l}{2}) \right) - \theta \left(t - (|x| + \frac{l}{2}) \right) \right] \quad (71)$$

This is because, when $t = -|x| + \frac{l}{2}$, the left moving partner of the entangled pair goes outside the interval, and when $t = |x| + \frac{l}{2}$ the right moving partner goes outside the interval.

Similarly, the contribution of the quasi-particles outside the interval A is

$$s_A^{(2)}(|x|, t) = \frac{c\pi}{6\beta} \left[\theta \left(t - (|x| - \frac{l}{2}) \right) - \theta \left(t - (|x| + \frac{l}{2}) \right) \right] \quad (72)$$

The total entanglement entropy $S_A(l, t)$ for the interval A is then given by

$$S_A(l, t) = 2 \int_{\frac{l}{2}}^{\infty} s_A^{(2)}(|x|, t) d|x| + 2 \int_0^{\frac{l}{2}} s_A^{(1)}(|x|, t) d|x|. \quad (73)$$

Here we incorporate the factor 2 to include the contribution of $x > 0$ region. Performing the integral we get

$$S_A(l, t) = \frac{2c\pi t}{3\beta} \theta\left(\frac{l}{2} - t\right) + \frac{c\pi l}{3\beta} \theta\left(t - \frac{l}{2}\right). \quad (74)$$

which gives us the result from a CFT calculation [7, 8].

5.2 The evolution of entanglement entropy in the presence of boundaries

We would now like to discuss the time evolution of the entanglement entropy in the presence of the boundaries. The new physics in this case comes from the reflection of the quasiparticles off the boundary walls. The entanglement entropy consists of two contributions. One is the contribution from the inside of the interval, and the other is the contribution from the outside of the interval. As we will see below the form of the each contribution is further classified by the ratio $\frac{l}{L}$ of size of the interval l to the size of the total system L .

Let us consider the motion of the left moving and the right moving quasiparticles which are located inside the interval A , say $-|x| \in A$ at the initial time $t = 0$. The left mover goes outside A at $t = \frac{l}{2} - |x|$, then it bounces off the boundary wall at $t = \frac{l}{2} - |x|$, and becomes a right mover. When $t = L - |x| - \frac{l}{2}$, it enters the interval A again. Similarly the right mover goes outside the interval A at $t = \frac{l}{2} + |x|$, bounces off the boundary wall at $\frac{l}{2} + |x|$, and enters the interval again at $t = L + |x| - \frac{l}{2}$.

5.3 $\frac{l}{L} > \frac{1}{2}$

Let us consider the contribution of the quasiparticle pairs which are located in $[-(|x| + d|x|), -|x|]$ at the initial time $t = 0$ to the entanglement entropy when $\frac{l}{L} > \frac{1}{2}$. The contribution of those inside the interval depends on the precise value of $|x|$. For $|x| < \frac{L-l}{2}$, since $|x| + \frac{l}{2} < (L - |x| - \frac{l}{2})$,

$$\begin{aligned} s_A^{\text{in}(1)} &= \frac{c\pi}{6\beta} \left[\theta\left(t - \left(\frac{l}{2} - |x|\right)\right) - \theta\left(t - \left(\frac{l}{2} + |x|\right)\right) \right] \\ &+ \frac{c\pi}{6\beta} \left[\theta\left(t - \left(L - |x| - \frac{l}{2}\right)\right) - \theta\left(t - \left(L + |x| - \frac{l}{2}\right)\right) \right] \end{aligned} \quad (75)$$

When $\frac{L-l}{2} < |x| < \frac{l}{2}$, since $(L - |x| - \frac{l}{2}) < |x| + \frac{l}{2}$

$$s_A^{\text{in}(2)} = \frac{c\pi}{6\beta} \left[\theta \left(t - \left(\frac{l}{2} - |x| \right) \right) - \theta \left(t - \left(L - |x| - \frac{l}{2} \right) \right) \right] \\ + \frac{c\pi}{6\beta} \left[\theta \left(t - \left(\frac{l}{2} + |x| \right) \right) - \theta \left(t - \left(L + |x| - \frac{l}{2} \right) \right) \right] \quad (76)$$

The contribution of the quasiparticles located outside the interval is

$$s_A^{\text{out}} = \frac{c\pi}{6\beta} \left[\theta \left(t - \left(|x| - \frac{l}{2} \right) \right) - \theta \left(t - \left(L - |x| - \frac{l}{2} \right) \right) \right] \\ + \frac{c\pi}{6\beta} \left[\theta \left(t - \left(\frac{l}{2} + |x| \right) \right) - \theta \left(t - \left(L + |x| - \frac{l}{2} \right) \right) \right] \quad (77)$$

The total entanglement entropy is then given by integrating all contribution of the quasiparticles.

$$S_A(l, t) = 2 \int_0^{\frac{L-l}{2}} s_A^{\text{in}(1)} d|x| + \int_{\frac{L-l}{2}}^{\frac{l}{2}} S_A^{\text{in}(2)}(|x|, t) + \int_{\frac{l}{2}}^{\frac{L}{2}} s_A^{\text{out}}(|x|, t) d|x| \quad (78)$$

The form of the integral of $s_A^{\text{in}(2)}$ depends on whether $\frac{l}{L} > \frac{3}{4}$ or not. The sum of the remaining two terms also depends on the size of the interval, ie $\frac{l}{L} > \frac{3}{4}$, $\frac{3}{4} > \frac{l}{L} > \frac{2}{3}$ or $\frac{2}{3} > \frac{l}{L} > \frac{1}{2}$. At the end of the day, these different cases give the same net entanglement entropy.

$$S_A(l, t) = \frac{\pi c}{6\beta} \times \begin{cases} 2t, & (0 < t < \frac{L-l}{2}) \\ 2t - L, & (\frac{L-l}{2} < t < \frac{2L+l}{2}) \\ L - l, & (\frac{L-l}{2} < t < \frac{l}{2}) \\ L - l, & (\frac{2L+l}{2} < t < \frac{2L-l}{2}), \\ -2t + L, & (\frac{l}{2} < t < \frac{L}{2}) \\ -2t + 2L, & (\frac{L+l}{2} < t < L) \end{cases}$$

In figure 7, we plot the EE obtained above from the quasiparticle picture and compare it to the holographic result. It is clear that the comparison works rather well.

It is important to note that in this case $l > \frac{L}{2}$, and the entanglement entropy is not thermalized at any time, i.e. it does not become proportional to the interval size l .

5.4 $\frac{l}{L} < \frac{1}{2}$

The contribution from inside the interval is now given by

$$s_A^{\text{in}} = \frac{c\pi}{6\beta} \left[\theta \left(t - \left(\frac{l}{2} - |x| \right) \right) - \theta \left(t - \left(\frac{l}{2} + |x| \right) \right) \right] \\ + \frac{c\pi}{6\beta} \left[\theta \left(t - \left(L - |x| - \frac{l}{2} \right) \right) - \theta \left(t - \left(L + |x| - \frac{l}{2} \right) \right) \right] \quad (79)$$

The contribution of the region $\frac{l}{2} < |x| < \frac{L-l}{2}$ is

$$s_A^{\text{out}(1)} = \frac{c\pi}{6\beta} \left[\theta \left(t - (|x| - \frac{l}{2}) \right) - \theta \left(t - (|x| + \frac{l}{2}) \right) \right] + \frac{c\pi}{6\beta} \left[\theta \left(t - (L - |x| + \frac{l}{2}) \right) - \theta \left(t - (L + |x| - \frac{l}{2}) \right) \right] \quad (80)$$

The contribution of the region $\frac{L-l}{2} < |x| < \frac{L}{2}$ is

$$s_A^{\text{out}(1)} = \frac{c\pi}{6\beta} \left[\theta \left(t - (|x| - \frac{l}{2}) \right) - \theta \left(t - (|x| + \frac{l}{2}) \right) \right] + \frac{c\pi}{6\beta} \left[\theta \left(t - (L - |x| + \frac{l}{2}) \right) - \theta \left(t - (L + |x| - \frac{l}{2}) \right) \right] \quad (81)$$

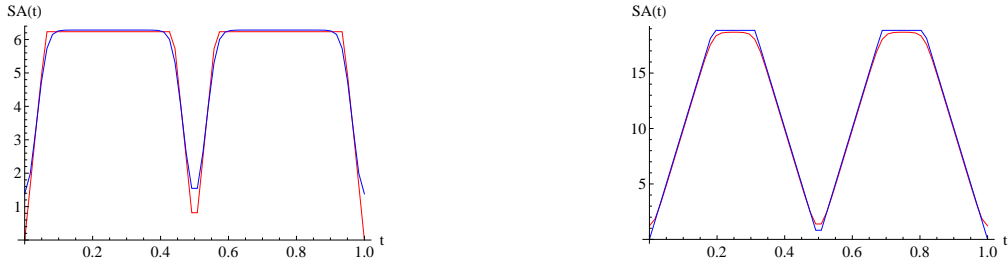


Figure 7: Plot of the time evolution of entanglement entropy in the quench in the high temperature regime (blue). We also plot the evolution of the entanglement entropy expected from the quasiparticle picture (red). We take $L = 1, \beta = \frac{1}{8}, l = \frac{1}{8}$ (left panel), $l = \frac{3}{8}$ (right panel).

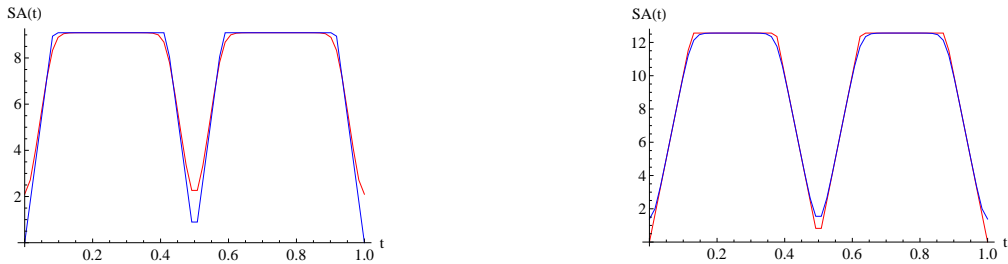


Figure 8: Plot of the time evolution of entanglement entropy in the quench in the high temperature regime (blue). We also plot the evolution of the entanglement entropy expected from the quasiparticle picture (red). We take $L = 1, \beta = \frac{1}{8}, l = \frac{5}{8}$ (left panel), $l = \frac{6}{8}$ (right panel).

Combining everything, the total EE is

$$S_A(l, t) = \frac{\pi c}{6\beta} \times \begin{cases} 2t, & (0 < t < \frac{l}{2}) \\ 2t - L, & (\frac{l}{2} < t < \frac{L+l}{2}) \\ l, & (\frac{l}{2} < t < \frac{L-l}{2}) \\ l, & (\frac{L+l}{2} < t < \frac{2L-l}{2}), \\ -2t + L, & (\frac{L-l}{2} < t < \frac{l}{2}) \\ -2t + 2L, & (\frac{2L-l}{2} < t < L) \end{cases}$$

As we can see, this behavior of the entanglement entropy is very similar to that of global quenches for infinite spatial size (74). This is natural because it takes a while until the reflections off the walls start affecting the entanglement entropy when the size of the subsystem A is small. As a result the entanglement entropy is thermalized when $\frac{l}{2} \leq t \leq \frac{L-l}{2}$. This is expected from the analysis of [9]. When $t \geq \frac{L-l}{2}$, it starts decreasing, leading to the ‘revival’ behavior discussed in this paper.

6 Conclusion

In this paper we have explored the properties of single-interval entanglement entropy (EE) in the presence of spatial boundaries. The distinguishing feature arising from such boundaries is the appearance of time-periodicity of the observables, arising from a bulk geometry which is a quotient of the AdS-Poincaré spacetime. The periodicity of the entanglement entropy can be understood in terms of a periodic motion of geodesic end-points. Another feature, for quench states corresponding²² to high temperatures, is the appearance of thermalization with universal exponents, followed by a revival [9, 27]. For quenches corresponding to intermediate or low temperatures, there is an apparent puzzle: the CFT EE depends on a four-point function which does not factorize and is hence non-universal; the holographic result however does not depend on details of the CFT except for the central charge c . We apply recent large- c techniques to resolve this puzzle. The large c limit of the CFT EE becomes universal and exactly matches the holographic computation at all temperatures. It would be interesting to see, following [58], whether corrections to the leading large c limit are captured by subdominant saddle points in the bulk.

In this paper, we have particularized to quenches to critical theories and modelled the quenched state by a Calabrese-Cardy (CC) type state [7, 8]. It would be interesting to (a) generalize our results to more general states with higher chemical potentials as discussed in [10], (b) explore realistic quenches with boundaries in the limit of fast ramping speed (some interesting issues have recently been raised in this context in [43, 44]) and (c) relate our results to the study of spatial boundaries in non-conformal theories (see, e.g. [59]). The presence of spatial boundaries can be regarded as a model for impurities or defects in a one-dimensional lattice. It would be interesting to relate some of our results to experimental situations.

An issue which has not been explored in detail in this paper, and is currently under investigation, is the precise nature of the bulk geometry found here. In particular, we would

²²In the sense of footnote 5.

like to understand the geometrical interpretation of the approximate thermalization of the one-point function and EE and subsequent revival. These issues have been commented upon in [27, 31]; however the explicit bulk metric we have found should shed more light on this issue. It is also interesting to see if the phenomenon of revival has a bearing on the issue of stability of the AdS geometry discussed in, e.g. [60, 61, 62].²³ We hope to return to these issues shortly.

Acknowledgments

We thank Justin David, Tarun Grover, Shiraz Minwalla, Mukund Rangamani, and Tadashi Takayanagi for a number of illuminating discussions. G.M. would like to thank the lecturers and participants of the Advanced String School in Bangalore, India in June 2015, for many discussions. The work of T.U. was supported in part by the National Science Foundation under Grant No. NSF PHY-25915. The work of T.U. was supported by JSPS Postdoctoral Research Fellowship for Young Scientists and in part by JSPS Grant-in-Aid for JSPS Fellows, in the earlier stage of this work.

A Derivation of conformal maps

In this appendix, we discuss in more detail the conformal map mentioned in Section 2.1.

A.1 Map from the rectangle to the complex plane (Euclidean)

We consider a rectangle parametrized by

$$w = x + i\tau, \bar{w} = x - i\tau, x \in [-\frac{L}{2}, \frac{L}{2}], \tau \in [-\frac{\beta}{4}, \frac{\beta}{4}] \quad (82)$$

which we wish to map to the upper half plane

$$z = z_2 + iz_1, \bar{z} = z_2 - iz_1, z_1 \geq 0, z_2 \in \mathbb{R} \quad (83)$$

As mentioned in Section 2.1, such a map is given by the Christoffel-Schwarz transformation (4)

$$w(z) = A \int_0^z \frac{dz}{\sqrt{(z^2 - b^2)(z^2 - \frac{1}{b^2})}} + B, \quad (84)$$

²³We thank Shiraz Minwalla for discussions on this issue.

By definition this map satisfies the following conditions

$$\begin{aligned} w(b) &= \frac{L}{2} + i\frac{\beta}{4}, & w(-b) &= \frac{L}{2} - i\frac{\beta}{4} \\ w\left(\frac{1}{b}\right) &= -\frac{L}{2} + i\frac{\beta}{4}, & w\left(-\frac{1}{b}\right) &= -\frac{L}{2} - i\frac{\beta}{4} \end{aligned} \quad (85)$$

It is easy to see that β is given by ²⁴

$$\beta = 2i(w(-b) - w(b)) = -2iA \int_{-b}^b \frac{dz}{\sqrt{(z^2 - b^2)(z^2 - \frac{1}{b^2})}} = 4iA bK(b^4), \quad (86)$$

where $K(m)$ is the Elliptic K function

$$K(m) = \int_0^1 \frac{1}{\sqrt{(1-x^2)(1-mx^2)}}$$

Similarly

$$L = w(b) - w(1/b) = iA bK(1 - b^4)$$

The constant B can now be determined from, say, the first of the conditions (85). We get $B = L/2$. The map, therefore, is given by

$$w(z) = \frac{i\beta}{4K(b^4)} sn^{-1}\left(\frac{z}{b}, b^4\right) + \frac{L}{2} \quad (87)$$

where we have used the following result about the Jacobi sn function

$$\int_0^z \frac{dz}{\sqrt{(z^2 - b^2)(z^2 - \frac{1}{b^2})}} = sn^{-1}\left(\frac{z}{b}, b^4\right)$$

The inverse map is

$$z = b sn \left[\frac{4K(b^4)}{i\beta} \left(w - \frac{L}{2} \right), b^4 \right] \quad (88)$$

where we can regard b as determined from

$$\frac{\beta}{L} = \frac{4K(b^4)}{K(1 - b^4)} \quad (89)$$

The antiholomorphic map reads as

$$\bar{z} = b sn \left[-\frac{4K(b^4)}{i\beta} \left(\bar{w} - \frac{L}{2} \right), b^4 \right] \quad (90)$$

²⁴We have used the convention

$$\frac{1}{\sqrt{(z^2 - b^2)(z^2 - \frac{1}{b^2})}} = -\frac{1}{\sqrt{(b^2 - z^2)(\frac{1}{b^2} - z^2)}}$$

Periodicity properties: Note the periodicity properties

$$z(w) = z(w + 2L), \quad z(w) = z(w + i\beta) \quad (91)$$

and the parity property

$$z(w + i\beta/4) = -z(w - i\beta/4) \quad (92)$$

which follow from the following properties of the Jacobi sn function [63]

$$sn(u + 2K(m), m) = -sn(u, m) = sn(u - 2K(m), m), \quad sn(u + 2iK(1 - m), m) = sn(u, m)$$

Map from $\mathbb{T}^2 \rightarrow \mathbb{C}$: The above periodicity properties (91) imply that the map $w \rightarrow z(w)$ can be viewed from a complex torus to the complex plane:

$$\begin{aligned} \mathbb{T}^2 \ni w \mapsto z(w) &= b \operatorname{sn} \left(\frac{4K(b^4)}{i\beta} \left(w - \frac{L}{2} \right), b^4 \right) \in \mathbb{C}, \\ w \equiv x + i\tau, \quad x \in \left[-\frac{L}{2}, \frac{3L}{2} \right], \quad \tau \in \left[-\frac{\beta}{4}, \frac{3\beta}{4} \right], \quad z &= z_2 + iz_1, \quad z_1, z_2 \in \mathbb{R} \end{aligned} \quad (93)$$

Here the torus is represented as a rectangle (whose opposite sides are to be identified). The earlier rectangle (82) is the bottom left ‘quadrant’ of this larger rectangle.

We should note here that the rectangle (82) (or rather the Lorentzian continuation of that) is the appropriate geometry for the quench problem, whereas the torus described above is the appropriate geometry for a thermal problem (where we have a periodicity in the imaginary time).

Large L limit: To see this limit, we note the following small m behaviour [63]

$$K(1 - m) \approx \frac{1}{2} \ln(16/m) + O(m), \quad K(m) = \pi/2 + O(m) \quad (94)$$

Thus, the large L limit corresponds to small b , with

$$\frac{\beta}{L} = \frac{4K(b^4)}{K(1 - b^4)} \approx \frac{\pi}{\ln(2/b)} + O(b^4)$$

Using (94) and

$$\begin{aligned} sn(u, m) &= \sin(u) - \frac{1}{4}m(u - \sin u \cos u) \cos u + O(m^2), \\ \sin(u/i) &= -i \sinh(u) \end{aligned} \quad (95)$$

we get from (88)

$$z \approx -ib \sinh \left(\frac{2\pi w}{\beta} - \ln(2/b) \right) \approx -ib \left(-\frac{1}{2} \right) \exp \left(-\frac{2\pi w}{\beta} + \ln(2/b) \right) \approx ie^{-2\pi w/\beta} \quad (96)$$

Hence, in this limit, we recover the map (8) from the cylinder to the complex plane with periodicity $w \equiv w + i\beta$. This periodicity is consistent with the (91) described above, in the limit where the aspect ratio $\beta/L \rightarrow 0$, which we can regard as an infinitely wide rectangle with width β whose opposite sides are identified (hence, a cylinder).

Low temperature limit: Using (94), and (89), we can find the following $b \rightarrow 1 - \epsilon$ behaviour

$$\frac{\beta}{L} \approx \frac{4}{\pi} \ln \left(\frac{16}{1 - b^4} \right)$$

which shows that $b \rightarrow 1 - \epsilon$ corresponds to the low temperature $\beta/L \rightarrow \infty$ limit. Using the formula

$$sn(iu, 1 - m) = i \tan(u) + O(m)$$

we can then easily derive the following low temperature limit of (88):

$$z(w) = i \cot \left(\frac{\pi}{4} + \frac{\pi w}{2L} \right) \quad (97)$$

This shows a periodicity $w \equiv w + 2L$, and is consistent with (91). The rectangle representing the torus (93) becomes in this limit an infinitely high strip of width L (with opposite sides identified, hence leading to a cylinder).

A.2 Lorentzian map

As we saw in the text, the map (88) described above helps convert observables computed in the UHP (83) to those in the Euclidean rectangle (82). As we indicated above, the same map also converts the complex plane to the torus (93). As described in Section 2.2, for real-time observables we are interested in a Lorentzian CFT on the manifold (16)

$$M_L = \mathbb{I} \times \mathbb{R} \ni x_{\pm} = x \mp t, \quad x \in \mathbb{I} = [-L/2, L/2], t \in \mathbb{R} \quad (98)$$

which describes the Wick-rotated rectangle (82) (it is an infinite strip of width L). We obtain them by analytically continuing CFT observables on the rectangle according to (15):

$$\tau = it, \rightarrow w = x + i\tau = x - t \equiv x_+, \bar{w} = x - i\tau = x + t \equiv x_- \quad (99)$$

For the holographic calculations described in Section 4, we need to *also* analytically continue the Euclidean z, \bar{z} plane to a Lorentzian plane $z_+, z_- \in \mathbb{R}^2$. Thus, we need an analytic continuation of the Euclidean map (88), (90). To do this, we note the identity [63]

$$sn(x/i, m) = -i \frac{sn(x, 1 - m)}{cn(x, 1 - m)} \quad (100)$$

Since under the analytic continuation (99), both w, \bar{w} become real, the above identity implies that both z and \bar{z} , become purely imaginary. We, therefore, define the following analytic continuation of the complex z -plane to the real plane

$$\begin{aligned} z &= iz_+, \quad \bar{z} = -iz_-, \\ z_{\pm} &= \begin{cases} -iz \equiv -i(z_2 + iz_1) = z_1 - z_0, \\ +i\bar{z} \equiv +i(z_2 - iz_1) = z_1 + z_0, \end{cases} \quad z_0 \equiv iz_2 \end{aligned} \quad (101)$$

where, z_{\pm} are given by the following functions (using (100))

$$z_{\pm} = f_{\pm}(x_{\pm}), \quad f_+(x) = f_-(x) = f(x) \equiv -b \frac{\operatorname{sn} \left[\frac{4K(b^4)}{\beta}(x - L/2), 1 - b^4 \right]}{\operatorname{cn} \left[\frac{4K(b^4)}{\beta}(x - L/2), 1 - b^4 \right]} \quad (102)$$

Note that in this map, $x_{\pm} = x \mp t$, with $x \in \mathbb{I} = [-L/2, L/2]$, $t \in \mathbb{R}$, whereas $z_{\pm} = z_1 \mp z_0$, $z_{0,1} \in \mathbb{R}$. Thus the above map is a map from the strip M_L (16) to the real plane \mathbb{R}^2 . The map is clearly conformal, which satisfies the property $dz_+ dz_- = f'(x_+) f'(x_-) dx_+ dx_-$. Note that the Lorentzian version of the high temperature map (96) becomes the Rindler map:

$$z_{\pm} = \exp\left(-\frac{2\pi x_{\pm}}{\beta}\right) \quad (103)$$

A.3 A different Euclidean map

We note that the map (88) is not the unique one that maps the rectangle to the UHP. We may consider, e.g., a different assignment of the corners to the boundary of the UHP:

$$\begin{aligned} w\left(-\frac{1}{b}\right) &= \frac{L_1}{2} - \frac{i\beta}{4}, & w\left(\frac{1}{b}\right) &= -\frac{L}{2} - \frac{i\beta}{4} \\ w(-b) &= \frac{L}{2} + \frac{i\beta}{4}, & w(b) &= -\frac{L}{2} + \frac{i\beta}{4} \end{aligned} \quad (104)$$

By using methods similar to Section A.1, we arrive at the following map

$$z = -b \operatorname{sn} \left[\frac{2K(b^4)}{L} \left(w - \frac{i\beta}{4} \right), b^4 \right] \quad (105)$$

where b now is given by

$$\frac{\beta}{L} = \frac{K(1 - b^4)}{K(b^4)}.$$

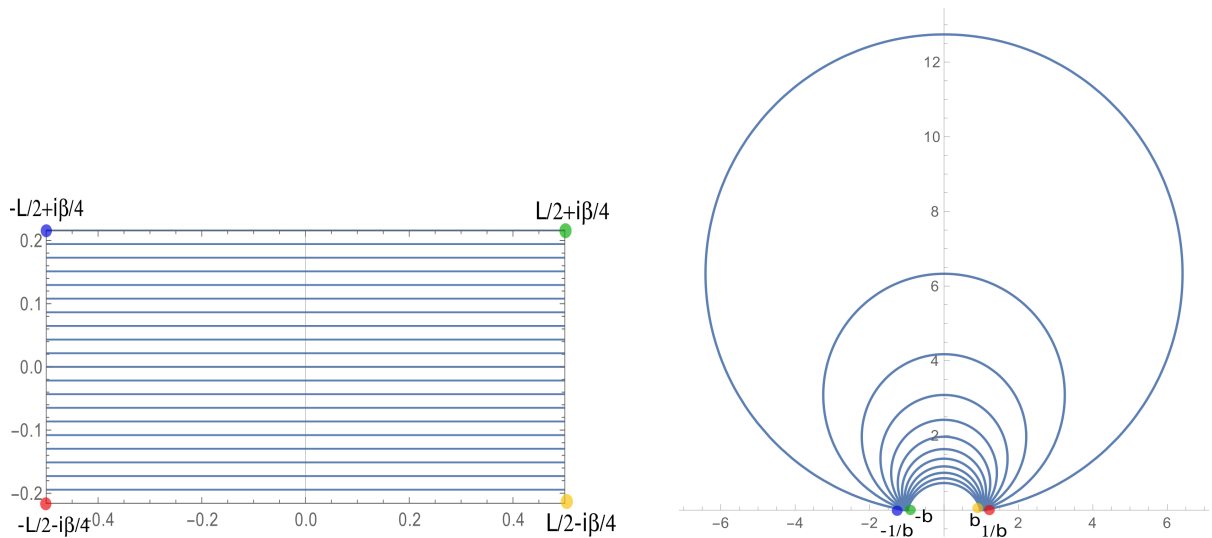


Figure 9: The second map between the upper half plane and the rectangle. The colour coding represents the mapping of the corners to the boundary of the UHP. See (88) and (87). The time evolution contours in the rectangle are mapped to the UHP as shown on the right. We have chosen $L = \beta = 1$. It is clear that this second map is roughly obtained from the first map by exchanging the horizontal and vertical axes of the complex plane.

The periodicity property of this map is the same as in (91). This map has the property that its low temperature limit is the standard cylinder map (with periodicity $2L$), as

$$z \approx i \exp\left(i \frac{\pi w}{L}\right) \quad (106)$$

The Euclidean map (105) cannot be analytically continued to a Lorentzian map as in (15). Here the continuation is $w = ix_+$, $\bar{w} = -ix_-$. This means that in the Euclidean theory we need to call $w =: \tau + ix$, $\bar{w} = \tau - ix$, and then analytically continue $\tau = it$ (here $x_{\pm} = x \pm t$). The accompanying continuation of the z -plane is $z = iz_+$, $\bar{z} = -iz_-$. As a simple check, note that (106) now becomes a real conformal map

$$z_{\pm} = \exp\left(-\frac{\pi x_{\pm}}{L}\right)$$

Comparing with (103), we can see that this second map is indeed related to the first map by an exchange of the horizontal and vertical axes, along with $\beta \leftrightarrow 2L$ (also, compare Figures 1 and 9).

B Decay rate in the high temperature limit

We will consider a one point function at the point $x = 0$ and at time t in the high temperature limit, where $\frac{L}{\beta} \gg \frac{t}{\beta} \gg 1$. Using the high temperature Lorentzian map (103), we find

that the Lorentzian continuation of the connected correlator $\langle \dots \rangle_{\mathbb{C}}$ in (11) gives

$$\left(\frac{(z_+ - z_-)}{b} \right)^{-2h} \simeq 2^{2h} \exp\left(-\frac{2\pi}{\beta}(2h)\left(t + \frac{L}{2}\right)\right) \quad (107)$$

The Jacobian terms in (11) become

$$\left(\frac{z'_+(x_+)z'_-(x_-)}{b} \right)^h \simeq \left(\frac{2\pi}{\beta}\right)^{2h} 2^{-2h} \left(\exp\left(\frac{4\pi t}{\beta}\right) + \exp\left(\frac{2\pi L}{\beta}\right) \right)^h \quad (108)$$

In the limit $\frac{L}{2\beta} \gg \frac{t}{\beta}$, the second term in the above expression dominates over the first. Combining the above two expressions, we get,

$$\langle \phi(w, \bar{w}) \rangle_{\text{rect}} \simeq \left(\frac{2\pi}{\beta}\right)^{2h} \exp\left(-\frac{4\pi h}{\beta}t\right) \quad (109)$$

Thus, the decay rate of the one point function in the limit $\frac{L}{\beta} \gg \frac{t}{\beta} \gg 1$ matches exactly with the decay rate obtained in [9] and [10] in the case of an infinite strip ($L \rightarrow \infty$).

C The BTZ and the global AdS metric

We will work out the metric (57) in case the maps $f_{\pm}(x_{\pm})$ are given by the non-compact limit $L \rightarrow \infty$ limit (8) and the low temperature $\beta \rightarrow \infty$ limits (9) of the general transformation (6).²⁵

Large L : BTZ Using the map (8) we first find that

$$L_+ = L_- \equiv \mathbf{L} = 4\pi^2/\beta^2 \quad (110)$$

which is consistent with (59) and (20). This allows us to write the map (8) as

$$z_{\pm} = f_{\pm}(x_{\pm}) = \exp[-\sqrt{\mathbf{L}}x_{\pm}] \quad (111)$$

The denominator D in (56) becomes

$$D = \mathbf{L} (\mathbf{L}z^2 + 4) e^{-2\sqrt{\mathbf{L}}x}, \quad (112)$$

²⁵ We must distinguish between (a) the non-compact limit $L \rightarrow \infty$ and (b) the high temperature limit $\beta \rightarrow 0$, although in both cases the aspect ratio $L/\beta \rightarrow \infty$. The difference is that in (a), ratios such as $\beta/L, x_{\pm}/L, l/L \rightarrow 0$ while ratios such as $x_{\pm}/\beta, l/\beta$ are not scaled, whereas in (b) ratios such $L/\beta, x_{\pm}/\beta, l/\beta \rightarrow \infty$, while $x_{\pm}/L, l/L$ are not scaled. In other words, in (a) only $L \rightarrow \infty$ and all other length scales are held fixed, while in (b) only $\beta \rightarrow 0$ and all other length scales are held fixed. Similarly limits of (c) low temperature $\beta \rightarrow \infty$ (where L, x_{\pm}, l are held fixed) and (d) small system size $L \rightarrow 0$ (where β, x_{\pm}, l are held fixed), are different. In this section we consider the limits (a) and (c).

The ‘large diffeomorphism’ (56) in this case is, therefore, given by

$$z_+ = f(x_+) \equiv \frac{e^{-\sqrt{\mathbf{L}}x_+} (4 - \mathbf{L}z^2)}{\mathbf{L}z^2 + 4}, \quad z_- = f(x) \zeta = \frac{4z\sqrt{\mathbf{L}}e^{-\sqrt{\mathbf{L}}(x_-+x_+)}}{\mathbf{L}z^2 + 4} \quad (113)$$

The resulting metric (57), turns out to be (see [39, 17, 18] for more details)

$$ds^2 = \frac{dz^2}{z^2} - \frac{(\mathbf{L}z^2 - 4)^2}{16z^2} dt^2 + \frac{(\mathbf{L}z^2 + 4)^2}{16z^2} dx^2, \quad (114)$$

which represents a BTZ black hole with horizon at

$$z_h = 2/\sqrt{\mathbf{L}} \quad (115)$$

In the large L limit the size of the spatial cycle effectively becomes decompactified; thus the above metric represents a BTZ black string. Thus, the BTZ black string is the bulk dual of the CFT on the (analytically continued) cylinder, which, of course, is the Lorentzian equivalent of the statement that the Euclidean black string is the bulk dual of the thermal CFT which is represented by the Euclidean cylinder.

The low temperature limit: Global AdS In the limit $\beta \gg L$, we apply the map (9) to the transformation (56). Here we find that

$$L_+ = L_- \equiv \mathbf{L} = -\pi^2/L^2 \quad (116)$$

which is consistent with (59) and (21).

By going through similar steps as the above, we find the final form of the metric (57) as

$$ds^2 = \frac{dz^2}{z^2} - \frac{(\mathbf{L}z^2 + 4)^2}{16z^2} dt^2 + \frac{(\mathbf{L}z^2 - 4)^2}{16z^2} dx^2 \quad (117)$$

which represents global AdS, since it is the spatial cycle x which shrinks to zero size at $z = 2/\sqrt{\mathbf{L}}$.

References

- [1] M. Greiner, O. Mandel, T. Esslinger, T. W. Hansch, and I. Bloch, *Quantum phase transition from a superfluid to a mott insulator in a gas of ultracold atoms*, *Nature* **415** (2002) p. 39.
- [2] M. Rigol, V. Dunjko, and M. Olshanii, *Thermalization and its mechanism for generic isolated quantum systems*, *Nature* **452** (2008) pp. 854–858, [[arXiv:0708.1324](https://arxiv.org/abs/0708.1324)].

- [3] P. Calabrese, F. H. L. Essler, and M. Fagotti, *Quantum quench in the transverse field Ising chain: I. Time evolution of order parameter correlators*, *Journal of Statistical Mechanics: Theory and Experiment* **07** (2012) p. 07016, [arXiv:1204.3911].
- [4] S. Bhattacharyya and S. Minwalla, *Weak Field Black Hole Formation in Asymptotically AdS Spacetimes*, *JHEP* **0909** (2009) p. 034, [arXiv:0904.0464].
- [5] P. M. Chesler and L. G. Yaffe, *Horizon formation and far-from-equilibrium isotropization in supersymmetric Yang-Mills plasma*, *Phys. Rev. Lett.* **102** (2009) p. 211601, [arXiv:0812.2053].
- [6] V. Balasubramanian, A. Bernamonti, J. de Boer, N. Copland, B. Craps, E. Keski-Vakkuri, B. Muller, A. Schafer, M. Shigemori, and W. Staessens, *Holographic Thermalization*, *Phys. Rev.* **D84** (2011) p. 026010, [arXiv:1103.2683].
- [7] P. Calabrese and J. L. Cardy, *Entanglement entropy and quantum field theory*, *J.Stat.Mech.* **0406** (2004) p. P06002, [hep-th/0405152].
- [8] P. Calabrese and J. L. Cardy, *Evolution of entanglement entropy in one-dimensional systems*, *J.Stat.Mech.* **0504** (2005) p. P04010, [cond-mat/0503393].
- [9] J. Cardy, *Thermalization and Revivals after a Quantum Quench in Conformal Field Theory*, *Phys.Rev.Lett.* **112** (2014) p. 220401, [arXiv:1403.3040].
- [10] G. Mandal, R. Sinha, and N. Sorokhaibam, *Thermalization with chemical potentials, and higher spin black holes*, arXiv:1501.0458.
- [11] J. Cardy, *Quantum Quenches to a Critical Point in One Dimension: some further results*, *J. Stat. Mech.* **1602** (2016), no. 2 p. 023103, [arXiv:1507.0726].
- [12] G. T. Horowitz and V. E. Hubeny, *Quasinormal modes of AdS black holes and the approach to thermal equilibrium*, *Phys.Rev.* **D62** (2000) p. 024027, [hep-th/9909056].
- [13] H. Casini, H. Liu, and M. Mezei, *Spread of entanglement and causality*, arXiv:1509.0504.
- [14] T. Hartman and J. Maldacena, *Time Evolution of Entanglement Entropy from Black Hole Interiors*, *JHEP* **1305** (2013) p. 014, [arXiv:1303.1080].
- [15] P. Caputa, G. Mandal, and R. Sinha, *Dynamical Entanglement Entropy with Angular Momentum and U(1) Charge*, *JHEP* **1311** (2013) p. 052, [arXiv:1306.4974].
- [16] S. Sotiriadis and J. Cardy, *Inhomogeneous quantum quenches*, *Journal of Statistical Mechanics: Theory and Experiment* **11** (Nov., 2008) p. 3, [arXiv:0808.0116].
- [17] T. Ugajin, *Two dimensional quantum quenches and holography*, arXiv:1311.2562.

- [18] G. Mandal, R. Sinha, and N. Sorokhaibam, *The inside outs of AdS(3)/CFT(2): Exact AdS wormholes with entangled CFT duals*, *JHEP* **1501** (2014) p. 036, [arXiv:1405.6695].
- [19] C. T. Asplund, A. Bernamonti, F. Galli, and T. Hartman, *Holographic Entanglement Entropy from 2d CFT: Heavy States and Local Quenches*, *JHEP* **1502** (2015) p. 171, [arXiv:1410.1392].
- [20] P. Caputa, M. Nozaki, and T. Takayanagi, *Entanglement of local operators in large-N conformal field theories*, *PTEP* **2014** (2014) p. 093B06, [arXiv:1405.5946].
- [21] C. T. Asplund and A. Bernamonti, *Mutual information after a local quench in conformal field theory*, *Phys. Rev.* **D89** (2014), no. 6 p. 066015, [arXiv:1311.4173].
- [22] A. F. Astaneh and A. E. Mosaffa, *Quantum Local Quench, AdS/BCFT and Yo-Yo String*, *JHEP* **05** (2015) p. 107, [arXiv:1405.5469].
- [23] P. J. Fermi E. and U. S., *Studies of nonlinear problems*. University of Chicago Press, 1955. Los Alamos report LA-1940, published later in *Collected Papers of Enrico Fermi*, E. Segr (Ed.).
- [24] T. Dauxois and S. Ruffo, *Fermi-Pasta-Ulam nonlinear lattice oscillations*, . Scholarpedia article.
- [25] B. Rink, *Fermi Pasta Ulam systems (FPU): mathematical aspects*, . Scholarpedia article.
- [26] T. Takayanagi and T. Ugajin, *Measuring Black Hole Formations by Entanglement Entropy via Coarse-Graining*, *JHEP* **1011** (2010) p. 054, [arXiv:1008.3439].
- [27] K. Kuns and D. Marolf, *Non-Thermal Behavior in Conformal Boundary States*, *JHEP* **1409** (2014) p. 082, [arXiv:1406.4926].
- [28] W.-Z. Guo and S. He, *Rnyi entropy of locally excited states with thermal and boundary effect in 2D CFTs*, *JHEP* **1504** (2015) p. 099, [arXiv:1501.0075].
- [29] E. da Silva, E. Lopez, J. Mas, and A. Serantes, *Collapse and Revival in Holographic Quenches*, *JHEP* **1504** (2015) p. 038, [arXiv:1412.6002].
- [30] D. Engelhardt, *Quench Dynamics in Confined 1+1-Dimensional Systems*, arXiv:1502.0267.
- [31] J. de Boer and D. Engelhardt, *Comments on Thermalization in 2D CFT*, arXiv:1604.0532.

- [32] J. Cardy, *Quantum Revivals in Conformal Field Theories in Higher Dimensions*, [arXiv:1603.0826](#).
- [33] J. Abajo-Arrastia, E. da Silva, E. Lopez, J. Mas, and A. Serantes, *Holographic Relaxation of Finite Size Isolated Quantum Systems*, *JHEP* **1405** (2014) p. 126, [[arXiv:1403.2632](#)].
- [34] A. Karch and L. Randall, *Locally localized gravity*, *JHEP* **0105** (2001) p. 008, [[hep-th/0011156](#)].
- [35] O. DeWolfe, D. Z. Freedman, and H. Ooguri, *Holography and defect conformal field theories*, *Phys.Rev.* **D66** (2002) p. 025009, [[hep-th/0111135](#)].
- [36] T. Takayanagi, *Holographic Dual of BCFT*, *Phys.Rev.Lett.* **107** (2011) p. 101602, [[arXiv:1105.5165](#)].
- [37] M. Fujita, T. Takayanagi, and E. Tonni, *Aspects of AdS/BCFT*, *JHEP* **1111** (2011) p. 043, [[arXiv:1108.5152](#)].
- [38] M. Nozaki, T. Takayanagi, and T. Ugajin, *Central Charges for BCFTs and Holography*, *JHEP* **1206** (2012) p. 066, [[arXiv:1205.1573](#)].
- [39] M. M. Roberts, *Time Evolution of Entanglement Entropy from a Pulse*, *JHEP* **1212** (2012) p. 027, [[arXiv:1204.1982](#)].
- [40] T. Hartman, *Entanglement Entropy at Large Central Charge*, [arXiv:1303.6955](#).
- [41] A. L. Fitzpatrick, J. Kaplan, and M. T. Walters, *Universality of Long-Distance AdS Physics from the CFT Bootstrap*, *JHEP* **1408** (2014) p. 145, [[arXiv:1403.6829](#)].
- [42] S. Leichenauer and M. Moosa, *Entanglement Tsunami in (1+1)-Dimensions*, *Phys. Rev.* **D92** (2015) p. 126004, [[arXiv:1505.0422](#)].
- [43] S. R. Das, D. A. Galante, and R. C. Myers, *Universality in fast quantum quenches*, *JHEP* **1502** (2015) p. 167, [[arXiv:1411.7710](#)].
- [44] S. R. Das, D. A. Galante, and R. C. Myers, *Universal scaling in fast quantum quenches in conformal field theories*, *Phys.Rev.Lett.* **112** (2014) p. 171601, [[arXiv:1401.0560](#)].
- [45] G. Mandal, S. Paranjape, and N. Sorokhaibam, *Thermalization in 2D critical quench and UV/IR mixing*, [arXiv:1512.0218](#).
- [46] J. L. Cardy, *Conformal Invariance and Surface Critical Behavior*, *Nucl.Phys.* **B240** (1984) pp. 514–532.

- [47] A. B. Zamolodchikov, *Conformal symmetry in two-dimensional space: Recursion representation of conformal block*, *Theor. Math. Phys* (1987) p. 1088.
- [48] J. M. Magn, D. Melnikov, and M. R. O. Silva, *Black Holes in AdS/BCFT and Fluid/Gravity Correspondence*, *JHEP* **11** (2014) p. 069, [arXiv:1408.2580].
- [49] J. D. Brown and M. Henneaux, *Central Charges in the Canonical Realization of Asymptotic Symmetries: An Example from Three-Dimensional Gravity*, *Commun.Math.Phys.* **104** (1986) pp. 207–226.
- [50] M. Banados, *Three-Dimensional Quantum Geometry and Black Holes*, hep-th/9901148.
- [51] T. Regge and C. Teitelboim, *Role of Surface Integrals in the Hamiltonian Formulation of General Relativity*, *Annals Phys.* **88** (1974) p. 286.
- [52] S. Wadia, *Canonical Quantization of Non-Abelian Gauge Theory in the Schrodinger Picture: Applications to Monopoles and Instantons*, *Ph.D. Thesis* (1979).
- [53] V. Balasubramanian and P. Kraus, *A Stress Tensor for Anti-de Sitter Gravity*, *Commun.Math.Phys.* **208** (1999) pp. 413–428, [hep-th/9902121].
- [54] T. Faulkner, *The Entanglement Renyi Entropies of Disjoint Intervals in AdS/CFT*, arXiv:1303.7221.
- [55] A. Lewkowycz and J. Maldacena, *Generalized gravitational entropy*, *JHEP* **1308** (2013) p. 090, [arXiv:1304.4926].
- [56] S. Ryu and T. Takayanagi, *Holographic derivation of entanglement entropy from AdS/CFT*, *Phys.Rev.Lett.* **96** (2006) p. 181602, [hep-th/0603001].
- [57] V. E. Hubeny, M. Rangamani, and T. Takayanagi, *A Covariant holographic entanglement entropy proposal*, *JHEP* **0707** (2007) p. 062, [arXiv:0705.0016].
- [58] A. L. Fitzpatrick, J. Kaplan, D. Li, and J. Wang, *On Information Loss in AdS₃/CFT₂*, arXiv:1603.0892.
- [59] F. Iglói and Y.-C. Lin, *Finite-size scaling of the entanglement entropy of the quantum Ising chain with homogeneous, periodically modulated and random couplings*, *Journal of Statistical Mechanics: Theory and Experiment* **6** (June, 2008) p. 4, [arXiv:0803.3610].
- [60] P. Bizon and A. Rostworowski, *On weakly turbulent instability of anti-de Sitter space*, *Phys.Rev.Lett.* **107** (2011) p. 031102, [arXiv:1104.3702].

- [61] O. J. Dias, G. T. Horowitz, and J. E. Santos, *Gravitational Turbulent Instability of Anti-de Sitter Space*, *Class.Quant.Grav.* **29** (2012) p. 194002, [[arXiv:1109.1825](#)].
- [62] A. Buchel, S. L. Liebling, and L. Lehner, *Boson stars in AdS spacetime*, *Phys.Rev.* **D87** (2013), no. 12 p. 123006, [[arXiv:1304.4166](#)].
- [63] M. Abramowitz and I. Stegun, *Handbook of Mathematical Functions*. Dover Publications, 1965.